



THE UNIVERSITY *of* EDINBURGH

Edinburgh Research Explorer

An endosiRNA-Based Repression Mechanism Counteracts Transposon Activation during Global DNA Demethylation in Embryonic Stem Cells

Citation for published version:

Berrens, RV, Andrews, S, Spensberger, D, Santos, F, Dean, W, Gould, P, Sharif, J, Olova, N, Chandra, T, Koseki, H, von Meyenn, F & Reik, W 2017, 'An endosiRNA-Based Repression Mechanism Counteracts Transposon Activation during Global DNA Demethylation in Embryonic Stem Cells' *Cell Stem Cell*, vol. 21, no. 5, pp. 694-703.e7. DOI: 10.1016/j.stem.2017.10.004

Digital Object Identifier (DOI):

[10.1016/j.stem.2017.10.004](https://doi.org/10.1016/j.stem.2017.10.004)

Link:

[Link to publication record in Edinburgh Research Explorer](#)

Document Version:

Peer reviewed version

Published In:

Cell Stem Cell

General rights

Copyright for the publications made accessible via the Edinburgh Research Explorer is retained by the author(s) and / or other copyright owners and it is a condition of accessing these publications that users recognise and abide by the legal requirements associated with these rights.

Take down policy

The University of Edinburgh has made every reasonable effort to ensure that Edinburgh Research Explorer content complies with UK legislation. If you believe that the public display of this file breaches copyright please contact openaccess@ed.ac.uk providing details, and we will remove access to the work immediately and investigate your claim.



1 **An endosRNA-based repression mechanism counteracts transposon activation**
2 **during global DNA demethylation in embryonic stem cells**

3
4 Rebecca V Berrens^{1,2,6}, Simon Andrews¹, Dominik Spensberger¹, Fátima Santos^{1,2}, Wendy
5 Dean¹, Poppy Gould¹, Jafar Sharif³, Nelly Olova^{1,5}, Tamir Chandra^{1,5}, Haruhiko Koseki³,
6 Ferdinand von Meyenn¹ and Wolf Reik^{1,4}

7
8 ¹Epigenetics Programme, Babraham Institute, Cambridge, CB22 3AT, UK.

9 ²University of Cambridge, The Old Schools, Trinity Lane, Cambridge CB2 1TN, UK.

10 ³RIKEN Research Center for Allergy & Immunology, 1-7-22 Suehiro-cho, Tsurumi,
11 Yokohama, 230-0045 Kanagawa, Japan.

12 ⁴Wellcome Trust Sanger Institute, Hinxton, CB10 1SA, UK.

13 ⁵Present address: MRC Human Genetics Unit, MRC Institute of Genetics and Molecular
14 Medicine, Crewe Road, Edinburgh EH4 2XU, UK.

15 ⁶Lead Contact

16

17 Contact

18 rebecca.berrens@gmail.com, vonmeyenn@babraham.ac.uk, Wolf.reik@babraham.ac.uk

19 **Abstract**

20 Erasure of DNA methylation and repressive chromatin marks in the mammalian germline
21 leads to risk of transcriptional activation of transposable elements (TEs). Here, we used
22 mouse embryonic stem cells (ESCs) to identify an endosRNA-based mechanism involved in
23 suppression of TE transcription. In ESCs with DNA demethylation induced by acute deletion
24 of *Dnmt1*, we saw an increase in sense transcription at TEs, resulting in an abundance of
25 sense/antisense transcripts leading to high levels of ARGONAUTE2 (AGO2) bound small
26 RNAs. Inhibition of Dicer and Ago2 expression revealed that small RNAs are involved in an
27 immediate response to demethylation-induced transposon activation, while the deposition of
28 repressive histone marks follows as a chronic response. *In vivo*, we also found TE-specific
29 endosRNAs present during primordial germ cell development. Our results suggest that
30 antisense TE transcription is a 'trap' that elicits an endosRNA response to restrain acute
31 transposon activity during epigenetic reprogramming in the mammalian germline.

32

33 **Introduction**

34 Epigenetic reprogramming in the mammalian germ line is key for restoration of
35 developmental potency and occurs at the preimplantation stage of embryonic development
36 and during development of primordial germ cells (PGCs) (Reik and Surani, 2015). These
37 events lead to global DNA methylation and H3K9me2 erasure together with the transient
38 transcriptional activation of specific classes of transposable elements (TEs) (Hajkova et al.,
39 2008, Rowe and Trono, 2011). This raises fundamental questions about the regulation of TE
40 defence in the absence of repressive epigenetic marks.

41
42 TEs comprise ~50% of the mammalian genome and can be categorised into two major
43 classes: retrotransposons and DNA transposons (Lander et al., 2001). While most TEs in the
44 genome are inactive due to mutations and/or truncations, around 1-2% of long interspersed
45 nuclear elements (LINEs) and endogenous retroviruses (ERVs) remain able to
46 retrotranspose (Maksakova et al., 2006). Notably, the ERV family members Intracisternal A
47 Particles (IAPs) and Early Transposons (ETns) are the most active TEs in the murine
48 germline (Maksakova et al., 2006).

49
50 Due to their ability to retrotranspose, TEs are thought to play an important role in genome
51 evolution, but can also cause genetic diseases (Goodier and Kazazian, 2008). In order to
52 protect the genome from harmful mutations, regulatory mechanisms must be in place to limit
53 their transcription.

54
55 TE activity is controlled by multiple epigenetic mechanisms including DNA methylation,
56 repressive histone modifications, and small RNAs (Rowe and Trono, 2011). In somatic
57 tissues DNA methylation and H3K9me2/3 have been shown to be responsible for TE
58 silencing (Walsh et al., 1998, Hutnick et al., 2010). However in the germ line DNA
59 methylation and H3K9me2 are globally erased, while H3K9me3 is maintained and
60 H3K27me3 is redistributed (Iurlaro et al., 2017, Tang et al., 2016). Indeed deletion of the
61 H3K9me3 methyltransferase *Setdb1* leads to activation of IAPs during PGC development as
62 well as in mouse embryonic stem cells (ESCs) (Karimi et al., 2011, Maksakove et al., 2013).
63 Further, global demethylation of naïve ESCs results in transcriptional activation of TEs and
64 subsequent resilencing by a redistribution of repressive histone marks (Walter et al., 2016).

65
66 A number of studies have demonstrated that small RNAs may also act post transcriptionally
67 as a second-tier defence against TEs, particularly in the germline. In mouse oocytes,
68 microRNAs (miRNAs) and endogenous short-interfering RNAs (endosRNAs) that control TE
69 expression have been identified (Tam et al., 2008, Flemer et al., 2013, Watanabe et al., 2006)

70 and in the male germline PIWI-interacting small RNAs (piRNAs) can also control TE
71 expression (Aravin et al., 2008). In ESCs tRNA fragments have been recently described to
72 play a role in ERV translational control (Schorn et al., 2017).

73

74 In contrast to somatic cells, increased pervasive transcription across TEs was reported in
75 ESCs, suggesting that TEs may regulate transcription of long noncoding RNAs (Kelley and
76 Rinn, 2012). Intriguingly however, in yeast it was shown that genome-wide pervasive
77 transcription antisense to transposons leads to an RNA interference (RNAi) response as a
78 defence mechanism against TEs (Cruz and Houseley, 2014). Sense/antisense transcription
79 permits the production of double stranded RNA (dsRNA) triggering RNAi (Fire et al., 1998)
80 which has also been identified as a control mechanism of TEs (Robert et al., 2005).

81

82 Here we test the hypothesis that genic transcripts antisense to TEs serve as a trap for
83 transcriptional activation of TEs during global demethylation in mammals. Generation of
84 *Dicer* as well as *Ago2* conditional and constitutive knockout ESC lines in the background of a
85 *Dnmt1* conditional knockout (cKO) line allowed us to define an 'immediate' endosiRNA
86 dependent repressive response to TE activation and a subsequent 'chronic' response,
87 characterised by targeting of repressive histone modifications, to global demethylation.

88

89 Results

90 Acute *Dnmt1* deletion leads to TE demethylation in ESCs

91 Our experimental system recapitulates epigenetic reprogramming of early embryos and
92 PGCs *in vitro*. We used Cre mediated conditional *Dnmt1* deletion in ESCs (*Dnmt1* cKO)
93 (Sharif et al., 2016) and sampled DNA and RNA at several defined time points after *Dnmt1*
94 deletion for methylome, long and small transcriptome, as well as chromatin analyses (Figure
95 1A).

96
97 By whole genome bisulfite sequencing (WGBS-seq), we confirmed that acute deletion of
98 *Dnmt1* led to genome-wide demethylation from an initial 85% CpG methylation to 35% at day
99 3 after deletion, and 20% at day 6 after deletion with no further demethylation thereafter
100 (Figure 1B, S1A). The residual methylation can be attributed to the activity of the *de novo*
101 DNA methyltransferases (Lei et al., 1996). Upon *Dnmt1* cKO loss of methylation was in genic
102 and intergenic elements, CGIs as well as non-CGI promoters (Fig 1B). Characteristic
103 methylation profiles over gene bodies were reduced with the same kinetics as the rest of the
104 genome upon *Dnmt1* cKO (Figure S1B). Furthermore, low methylated regions (LMRs) and
105 active enhancers became demethylated (Fig S1C). Thus, this *in vitro* model results in
106 replication dependent global demethylation of the genome, which closely resembles the
107 dynamics of global reprogramming in early embryos and PGCs (von Meyenn et al., 2016).

108
109 To analyse TEs in WGBS-seq, RNA-seq and ChIP-seq data, we only considered uniquely
110 mapped reads and filtered out TEs overlapping the (+/- 2 kb) region surrounding genes.
111 While unique mapping might not capture all information about young TEs (as they lack the
112 increased sequence divergence of older TEs which makes unique mapping more efficient;
113 Lerat et al., 2003), this conservative approach allows us to be confident that mapped reads
114 can be definitively ascribed to specific TE subfamilies. Moreover, the filtering of the region
115 (+/- 2 kb) surrounding genes avoids ambiguity about the origin of TE expression from
116 promoters which are not their own (Figure S1D, [Data S1](#)).

117
118 Acute *Dnmt1* deletion led to hypomethylation of TEs at the same rate as the rest of the
119 genome (Figure 1B, S1E) with the exception of IAPs, RLTRs and MMERVK10C, which
120 preserved higher methylation levels (Figure S1F). Thus our experimental system also closely
121 recapitulates global demethylation dynamics of TEs *in vivo*, including the fact that IAPs are
122 relatively resistant to global demethylation (Seisenberger et al., 2012, Kobayashi et al.,
123 2013).

124

125 **Increased sense transcription of TEs upon hypomethylation combines with pervasive**
126 **antisense transcription**

127 Next, we performed total RNA sequencing (RNA-seq) upon acute *Dnmt1* deletion to examine
128 if demethylation led to transcriptional activation of TEs. Transcriptional activation was limited
129 to specific classes of ERVs (Figure 1C). We found TEs with increased transcription upon
130 hypomethylation that remained active over the whole time-course (MMERVK10C) as well as
131 TEs initially activated but notably subsequently re-silenced (e.g. IAPs and MERVLs).

132

133 In addition to TEs, a small number of genes became activated upon loss of DNA methylation
134 (Figure S1G, H), including the imprinted genes *Xlr3a*, *Mirg* and *Rian* (Table S1), consistent
135 with the known roles for methylation in regulation of these genes (Ferguson-Smith, 2011)
136 (Figure S1I). DNA hypomethylation did not result in ESC differentiation, as indicated by the
137 unaltered expression of the core pluripotency network (Figure S1J).

138

139 Interestingly, when quantifying reads overlapping with genes we found upon global
140 hypomethylation increased pervasive transcription in the antisense orientation to those
141 genes (Figure 1D). These pervasive antisense transcripts are in fact produced by
142 transcription of TEs that have integrated in an antisense orientation to the genes (Figure 1E).
143 Consistent with previous studies, high numbers of TEs were found to be preferentially
144 integrated in antisense orientation to genes (van de Lagemaat et al., 2006) (Figure S1K).

145

146 We next analysed the total RNA-seq data to determine whether both sense and antisense
147 transcription was detectable at sites of TE integration. Indeed, TE antisense transcription
148 was found in all TE families, with sense transcripts of members of the ERVs being
149 upregulated consistent with their activation in response to demethylation (Figure 1F). We
150 also included TEs which were not activated by hypomethylation, but instead are regulated in
151 a DICER dependent manner (see Figure 3E).

152

153 **Sense/antisense transcription of TEs correlates with AGO2 bound endosiRNAs**

154 The production of sense and antisense transcripts across TEs is expected to lead to
155 dsRNAs, which can subsequently induce an RNAi response and silence TEs post-
156 transcriptionally. These results suggest that TE expression may be sensed by pervasive
157 antisense transcription, thus constituting a TE 'trap' (Figure 2A). To test this hypothesis, we
158 performed small RNA-seq at defined time-points after *Dnmt1* deletion. The majority of small
159 RNAs were miRNAs (Figure S2A-C) and were expressed independently of DNA methylation,
160 with the exception of miRNAs from the imprinted *Dlk* and *Xlr3* loci (Figure S2D, E). Small
161 RNA quantitative real-time PCR (RT-qPCR) of mature miRNAs confirmed their methylation

162 dependent regulation (Figure S2F). The *Dlk* locus serves as an example of the genome-wide
163 response to acute *Dnmt1* deletion with the imprint control region (ICR) becoming
164 demethylated leading to transcriptional upregulation of the imprinted locus and embedded
165 miRNAs (Figure S2G).

166
167 Due to the short reads in small RNA-seq, we used TE consensus sequence mapping to
168 analyse global TE derived small RNAs. This method allows unambiguous alignment to
169 unique TE classes. Notably, we observed a substantial increase of small RNAs mapping to
170 IAP, MERVL and ETn upon *Dnmt1* deletion (Figure 2B), which in the case of IAPs mapped
171 across the whole length of the element (Figure 2C). Small RNAs mapping to L1MdGf and
172 MMERVK10C, respectively, were detected both in wild type (WT) and *Dnmt1* cKO ESCs
173 (Figure 2B).

174
175 The mammalian ARGONAUTE proteins (AGO) are critical components of the RNA induced
176 silencing complex (RISC). AGO2 can bind miRNAs as well as endogenous siRNAs
177 (endosRNAs) and has the ability to “slice” its targets (Doi et al., 2003). We performed AGO2
178 immunoprecipitation (IP) from *Dnmt1* cKO ESC at day 9 after deletion and analysed the
179 pulldown by small RNA-seq (Figure 2D). The AGO2-IP small RNA-seq libraries of both WT
180 and *Dnmt1* cKO ESCs were composed to 90% of known miRNAs, while 40% of the
181 remaining small RNAs mapped to TEs (Figure S2H, only *Dnmt1* cKO shown). This subset of
182 AGO2 bound small RNAs was 22 nucleotides (nts) long and mapped to sense and antisense
183 strands of TEs (Figure 2E); the small RNAs had 5' U-overhangs (Figure S2I) and formed
184 characteristic 5'-5' overlaps at nt 20, identifying them as *bona fide* endosRNAs (Figure S2J)
185 (Ghildiyal and Zamore, 2009). AGO2 bound endosRNAs mapping to MERVL and RLTR45
186 were expressed throughout the time-course while endosRNAs mapping to L1, IAP and ETn
187 or MMERVK10C were significantly enriched upon *Dnmt1* deletion (Figure 2F), suggesting
188 that functional endosRNAs against specific TE classes are generated during global
189 demethylation.

190
191 We also generated small RNA-seq libraries of E13.5 and E14.5 male and female PGCs and
192 found that ~10% of all 20-24 nt small RNAs mapped to TEs in both male and female E13.5
193 and E14.5 PGCs with small RNAs mapping to IAPEZ and L1MdGf particularly enriched in
194 E14.5 PGCs (Figure S2K-L). These small RNAs had the defining properties of endosRNAs
195 (Figure S2M-O), suggesting that a similar response to the one we have discovered in ESCs
196 also exists during global demethylation in the germ line *in vivo*.

197
198 **Key RNAi components are involved in the repression of specific TE classes**

219 To investigate whether the observed endosiRNAs were involved in restraining TE
220 expression, we knocked down key components of the endosiRNA and miRNA pathways in
221 *Dnmt1* cKO and monitored IAP expression by RT-qPCR. Upon knockdown of *Dicer* or *Ago2*,
222 both essential components of the RNAi pathway, IAP transcription was strongly upregulated,
223 while knockdown of *Dgcr8* (dispensable for endosiRNA function) had no effect on IAP
224 expression (Figure 3A). This suggests that TEs are controlled by functional endosiRNAs.

225
226 To examine the role of the RNAi pathway during global hypomethylation in more detail we
227 generated conditional *Dicer/Dnmt1* cDKO ESCs (Figure S3A), and carried out a number of
228 quality controls. Loss of *Dicer* activity was confirmed by loss of expression of mmu-miR-93,
229 while *Dicer* independent small nucleolar RNAs (snoRNAs) were still expressed (Figure S3A).
230 We generated total RNA-seq data from *Dicer/Dnmt1* cDKO ESCs and found increased
231 antisense transcripts in these cells, as seen earlier in the *Dnmt1* cKO ESCs (Figure S3B).
232 Furthermore, small RNA-seq of *Dicer/Dnmt1* cDKO ESCs showed a depletion of all miRNAs
233 (Figure S3C) and a loss of 21-24nt small RNAs mapping to all TEs as well as specifically to
234 L1MdGf and IAPEz (Figure 3B, S3D), which proves that the described small RNAs are
DICER dependent products.

235
236 Acute conditional deletion of both *Dicer* and *Dnmt1* together resulted in significantly higher
237 levels of transcription of IAPs by day 10 in comparison to those in *Dnmt1* cKO ESCs (Figure
238 3C). Importantly, there was no notable resilencing of IAP transcripts in *Dicer/Dnmt1* cDKO.
239 This demonstrates that DICER plays a role in the re-repression of IAPs upon global
240 hypomethylation. LINEs and major satellites (non-TE pericentric repeats), whilst not
241 upregulated upon *Dnmt1* deletion, were also dramatically upregulated following *Dicer*
242 deletion (Figure 3C). *Dicer/Dnmt1* cDKO ESCs started to show signs of cell death from day
243 12 after deletion, potentially as a result of TE mobilisation, as has been shown in constitutive
244 *Dicer* KO (Bodak et al., 2017).

245
246 We next asked whether deletion of RNAi components downstream of DICER would lead to a
247 similar response and generated conditional *Ago2/Dnmt1* cDKO ESCs (Figure S4G). While
248 we initially expected that *Ago2/Dnmt1* cDKO might show comparable results to the
249 *Dicer/Dnmt1* cDKO, we found that the deletion kinetics of *Ago2* KO in their respective ESC
250 lines were substantially slower (Figure S3E-G). Surprisingly however, we found that
251 transcriptional upregulation of TEs in the *Ago2/Dnmt1* cDKO was considerably blunted
252 (Figure 3D).

253
254

235 To gain deeper insights into the blunted TE expression, we constitutively deleted *Ago2* or
236 *Dicer* using CRISPR/Cas9 genome editing in the background of *Dnmt1* cKO ESCs (Figure
237 S5H-J). We first determined the effect of *Dicer* KO on genic and transposon transcription and
238 were able to identify TEs that were solely dependent on DICER for their silencing, such as
239 L1MdGf (Figure 3E, S3K-O).

240

241 We next performed a time-course of *Dnmt1* deletion in *Ago2* KO/*Dnmt1* cKO and in *Dicer*
242 KO/*Dnmt1* cKO and measured IAP expression by RT-qPCR. Notably, we found substantially
243 attenuated upregulation of IAPs upon *Dnmt1* deletion in both ESC lines, which was
244 confirmed by total RNA-seq (Figure 3D, S3O). These results indicate that in addition to DNA
245 methylation and RNAi, alternative TE silencing mechanisms can be recruited. While DICER
246 dependent mechanisms restrict the expression of specific TE classes upon deletion of
247 *Dnmt1*, ablation of the RNAi pathway prior to demethylation triggers the engagement of
248 another silencing mechanism. Since repressive histone marks have been shown to
249 contribute to TE repression in somatic tissues and in ESCs (Karimi et al., 2011, Maksakova
250 et al., 2006) we asked whether these might constitute the additional repressive mechanism
251 observed here.

252

253 **TE silencing by repressive histone marks**

254 To study the involvement of chromatin in TE regulation upon global hypomethylation, we
255 carried out ChIP-seq analyses of the repressive histone marks H3K9me2, H3K9me3 and
256 H3K27me3 at 4 and 8 days after deletion of *Dnmt1*, i.e. before and after transcriptional
257 upregulation of the relevant TE classes. Genome-wide distribution of the repressive histone
258 marks - H3K27me3, H3K9me2 and H3K9me3 - confirmed earlier studies (Iurlaro et al., 2017,
259 Tang et al., 2016) with H3K27me3 enrichment in gene bodies and H3K9me2/3 enrichment in
260 TEs (Figure S4A). Additionally, H3K27me3 was enriched in promoter regions but depleted at
261 transcription start sites (TSS) (Figure S4B,C). Upon *Dnmt1* deletion neither of these
262 repressive histone marks were redistributed genome-wide (Figure S4D).

263

264 However, DICER-independent MERVLs showed increased H3K27me3 deposition upon
265 *Dnmt1* deletion, recapitulating what has been reported in naïve hypomethylated ESCs
266 (Walter et al., 2016) (Figure 4A). We found H3K9me3 enrichment across IAPs independent
267 of DNA methylation levels, confirming previous results (Figure S4E,F) (Walter et al., 2016,
268 Sharif et al., 2016). Importantly, H3K27me3 and H3K9me2 deposition was found on IAPs 9
269 days after *Dnmt1* deletion, explaining why early, but not late, depletion of *Dicer* or *Ago2*
270 result in sustained TE expression. These results show that two repressive pathways are in
271 place to control TE expression in ESCs (Figure S4I), and, importantly, that they are

272 staggered in time, with an immediate RNAi response and a subsequent chronic chromatin
273 response.

274

275 To obtain insights into the attenuated IAP expression in *Dicer* KO/*Dnmt1* cKO, we performed
276 ChIP-seq of the same repressive histone marks. While we did not observe a genome-wide
277 redistribution of H3K27me3, H3K9me2 and H3K9me3 in the *Dicer* KO nor the *Dicer*
278 KO/*Dnmt1* cKO (Figure S4G,H), we observed a clear redistribution of repressive histone
279 marks over TEs in *Dicer* KO and in particular an enrichment of H3K27me3 and of H3K9me2
280 at IAPs. This was even further increased upon *Dnmt1* deletion (Figure 4B). Hence, acute
281 depletion of DICER during global demethylation abrogates re-silencing of IAPs whilst
282 constitutive deletion of *Dicer* instigates a repressive chromatin response in IAPs which
283 suppresses reactivation upon hypomethylation (Figure 4C).

284

285 **Discussion**

286 How TEs are controlled during global epigenetic reprogramming in the mammalian germline
287 is a highly relevant question. The present study provides to our knowledge the first evidence
288 of AGO2 bound endosiRNAs in ESCs during global DNA hypomethylation, which restrict TE
289 expression as judged by acute depletion of *Dicer* or *Ago2*. That we also detect DICER-
290 dependent endosiRNAs in PGCs indicates that it is likely that the described mechanism also
291 operates *in vivo*. This mechanism constitutes a first line of TE defence during epigenetic
292 reprogramming. A second line of defence is provided by chromatin targeting and retargeting,
293 presumably through the evolution of sequence specific recognition modules of TEs such as
294 zinc finger proteins (Rowe and Trono, 2011). Our work also indicates a link between these
295 systems; they are staggered in time and thus potentially connected.

296

297 Many TE families are associated with transcribed genes or lncRNAs in ESCs (Kelley and
298 Rinn, 2012). This provides the potential for sense/antisense transcription to occur when TEs
299 become demethylated, as observed here (Figure 1F). In oocytes, pseudogenes provide the
300 antisense strand to TEs to feed into an RNAi pathway (Tam et al., 2008) and TEs have been
301 shown to give rise to dsRNA in preimplantation embryos due to their bidirectional promoters
302 (Svoboda et al., 2004). Indeed, we found intragenic active TEs preferentially integrated in
303 antisense direction to the gene (Figure S1K). Previous studies had concluded that this could
304 prevent disruption of normal gene expression (van de Lagemaat et al., 2006). We suggest an
305 additional reason why this direction of insertion is evolutionarily favoured: it produces a
306 trapping system ('trap') for transposon activation during epigenetic reprogramming, in order
307 to tame newly invading TEs (Fig 2A).

308

309 Overlapping sense/antisense transcription feeds into an endosiRNA pathway regulated by
310 DICER and AGO2 to silence TEs. The generation of the two constitutive and conditional KO
311 ESCs in the background of the *Dnmt1* cKO allowed us to dissect the dynamics of TE control
312 during global hypomethylation, revealing an 'immediate' response which is characterised by
313 endosiRNAs and affected by acute depletion of *Dicer* or *Ago2*. This is followed by a 'chronic'
314 response which is defined by targeting of repressive histone modifications (particularly
315 H3K27me3 and H3K9me2) and occurs subsequent to the endosiRNA response in *Dnmt1*
316 cKO and *Dnmt1/Dicer* cDKO ESCs (Figure 4C). Intriguingly, non-acute depletion of *Dicer*
317 also instigates deposition of H3K27me3 and H3K9me2 independent of DNA demethylation,
318 suggesting that the two systems are linked. We suggest a mechanism of TE control by which
319 the 'immediate' endosiRNA response to global methylation erasure is followed by a 'chronic'
320 repressive chromatin response. Interestingly, the 'chronic' response is initiated by deletion of
321 *Dnmt1* as well as by abrogation of the 'immediate' defence. Therefore, the 'immediate' and

322 'chronic' responses are not only staggered in time but also appear mechanistically linked.
323 Unravelling the molecular underpinnings of this link will be an important topic of future work.

324

325 The specific response of IAPs and LINEs to loss of DICER may be explained by the fact that
326 they embody the most active retrotransposition competent TE copies in the mouse germline
327 (Maksakova et al., 2006) and are primarily guarded by endosiRNAs, with chromatin playing a
328 secondary role in their transcriptional restriction. Other TEs by contrast are primarily
329 controlled by chromatin redistribution upon global demethylation. The present study
330 highlights the exquisite variety and interplay of epigenetic modifications by which the
331 transcription of different TE families is regulated. Future work in this area, particularly with
332 high coverage long read sequencing, will hopefully allow the characterisation of
333 transcriptional and epigenetic regulation of individual TE copies in the genome.

334

335 We identified DICER as an important factor in small RNA dependent silencing of TEs.
336 Nonetheless, DICER-independent AGO2-bound small RNAs may also play a role in TE
337 silencing (Babiarz et al., 2008, Murchison et al., 2005). DICER-independent small RNAs
338 might also explain the repression of ETns, to which increasing amounts of AGO2-bound
339 small RNAs mapped, but which were not responsive to *Dicer* KO.

340

341 TEs benefit from transcriptional activation in the germ line but not in somatic cells (Haig,
342 2016). Hence one might speculate that they may regulate aspects of epigenetic
343 reprogramming in germ cells to their benefit. In this respect TEs may not be the sole
344 benefactors of their own mobilisation but it also impacts on creating novelty in the host
345 genome. Nevertheless unrestrained activation and transposition would presumably be
346 detrimental to the host genome, and hence a sophisticated balance of regulatory
347 mechanisms for TEs has evolved in the germ line, including the chromatin retargeting and
348 the endosiRNA pathway we report here.

349 **Author Contributions**

350 RVB conceived and designed the study, performed experiments, analysed data and wrote
351 the paper; SA analysed data; DS, WD, PG, JS and FS performed experiments; NO and TC
352 helped to design the project; HK provided supervision; FvM designed and supervised the
353 study and wrote the paper; WR conceived, designed and supervised the study and wrote the
354 paper.

355

356 **Acknowledgments**

357 We thank all members of the Reik lab for helpful discussions, Felix Krueger for bioinformatics
358 support, the sequencing facilities at Babraham Institute (BI) and Sanger Institute and the flow
359 cytometry facility at BI for support. We thank Jon Houseley, Andrea Schorn and Rob
360 Martienssen for helpful discussions, and Dónal O'Carroll for providing the AGO2 antibody
361 and sharing the AGO2 IP protocol. FvM was supported by the SNFS. RVB is funded by the
362 Gates Cambridge Trust. WR is supported by the BBSRC (BB/K010867/1), Wellcome Trust
363 (095645/Z/11/Z), EU BLUEPRINT, and EpiGeneSys. WR is a consultant and shareholder of
364 CEGX.

365

366

367 **References**

368 Aravin, A.A., Sachidanandam, R., Bourc'his, D., Schaefer, C., Pezic, D., Toth, K.F., Bestor,
369 T., and Hannon, G.J. (2008). A piRNA Pathway Primed by Individual Transposons Is Linked
370 to De Novo DNA Methylation in Mice. *Mol. Cell* *31*, 785–799.

371 Babiarz, J.E., Ruby, J.G., Wang, Y., Bartel, D.P., and Blelloch, R. (2008). Mouse ES cells
372 express endogenous shRNAs, siRNAs, and other Microprocessor-independent, Dicer-
373 dependent small RNAs. *Genes Dev.* *22*, 2773–2785.

374 Bernstein, E., Kim, S.Y., Carmell, M.A., Murchison, E.P., Alcorn, H., Li, M.Z., Mills, A.A.,
375 Elledge, S.J., Anderson, K.V., and Hannon, G.J. (2003). Dicer is essential for mouse
376 development. *Nat. Genet.* *35*, 287–287.

377 Bodak, M., Cirera-Salinas, D., Yu, J., Ngondo, R.P., and Ciaudo, C. (2017). Dicer, a new
378 regulator of pluripotency exit and LINE-1 elements in mouse embryonic stem cells. *FEBS*
379 *Open Bio* *7*, 204–220.

380 Chen, C., Morris, Q., and Mitchell, J.A. (2012). Enhancer identification in mouse embryonic
381 stem cells using integrative modeling of chromatin and genomic features. *BMC Genomics*
382 *13*, 152.

383 Creighton, M.P., Cheng, A.W., Welstead, G.G., Kooistra, T., Carey, B.W., Steine, E.J.,
384 Hanna, J., Lodato, M.A., Frampton, G.M., Sharp, P.A., et al. (2010). Histone H3K27ac
385 separates active from poised enhancers and predicts developmental state. *Proc. Natl. Acad.*
386 *Sci. U. S. A.* *107*, 21931–21936.

387 Doi, N., Zenno, S., Ueda, R., Ohki-Hamazaki, H., Ui-Tei, K., and Saigo, K. (2003). Short-
388 Interfering-RNA-Mediated Gene Silencing in Mammalian Cells Requires Dicer and eIF2C
389 Translation Initiation Factors. *Curr. Biol.* *13*, 41–46.

390 Ferguson-Smith, A.C. (2011). Genomic imprinting: the emergence of an epigenetic
391 paradigm. *Nat. Rev. Genet.* *12*, 565–575.

392 Fire, A., Xu, S., Montgomery, M.K., Kostas, S.A., Driver, S.E., and Mello, C.C. (1998). Potent
393 and specific genetic interference by double-stranded RNA in *Caenorhabditis elegans*. *Nature*
394 *391*, 806–811.

395 Flemr, M., Malik, R., Franke, V., Nejepinska, J., Sedlacek, R., Vlahovicek, K., and Svoboda,
396 P. (2013). A Retrotransposon-Driven Dicer Isoform Directs Endogenous Small Interfering
397 RNA Production in Mouse Oocytes. *Cell* *155*, 807–816.

398 Friedli, M., and Trono, D. (2015). The Developmental Control of Transposable Elements and
399 the Evolution of Higher Species. *Annu. Rev. Cell Dev. Biol.* *31*, 429–451.

400 Ghildiyal, M., and Zamore, P.D. (2009). Small silencing RNAs: an expanding universe. *Nat.*
401 *Rev. Genet.* *10*, 94–108.

402 Goodier, J.L., and Kazazian, H.H. (2008). Retrotransposons Revisited: The Restraint and
403 Rehabilitation of Parasites. *Cell* *135*, 23–35.

404 Haig, D. (2016). Transposable elements: Self-seekers of the germline, team-players of the
405 soma. *BioEssays* *38*, 1158–1166.

406 Hajkova, P., Ancelin, K., Waldmann, T., Lacoste, N., Lange, U.C., Cesari, F., Lee, C.,
407 Almouzni, G., Schneider, R., and Surani, M.A. (2008). Chromatin dynamics during epigenetic
408 reprogramming in the mouse germ line. *Nature* *452*, 877–881.

409 Han, B.W., Wang, W., Zamore, P.D., and Weng, Z. (2015). piPipes: a set of pipelines for
410 piRNA and transposon analysis via small RNA-seq, RNA-seq, degradome- and CAGE-seq,
411 ChIP-seq and genomic DNA sequencing. *Bioinformatics* *31*, 593–595.

412 Hutnick, L.K., Huang, X., Loo, T.-C., Ma, Z., and Fan, G. (2010). Repression of
413 Retrotransposal Elements in Mouse Embryonic Stem Cells Is Primarily Mediated by a DNA
414 Methylation-independent Mechanism. *J. Biol. Chem.* *285*, 21082–21091.

415 Illingworth, R.S., and Bird, A.P. (2009). CpG islands--'a rough guide'. *FEBS Lett.* *583*, 1713–
416 1720.

417 Iurlaro, M., von Meyenn, F., and Reik, W. (2017). DNA methylation homeostasis in human
418 and mouse development. *Curr. Opin. Genet. Dev.* *43*, 101–109.

419 Karimi, M.M., Goyal, P., Maksakova, I.A., Bilenky, M., Leung, D., Tang, J.X., Shinkai, Y.,
420 Mager, D.L., Jones, S., Hirst, M., et al. (2011). DNA Methylation and SETDB1/H3K9me3
421 Regulate Predominantly Distinct Sets of Genes, Retroelements, and Chimeric Transcripts in
422 mESCs. *Cell Stem Cell* *8*, 676–687.

423 Kelley, D.R., and Rinn, J.L. (2012). Transposable elements reveal a stem cell specific class
424 of long noncoding RNAs. *Genome Biol.* *13*, R107.

425 Kobayashi, H., Sakurai, T., Miura, F., Imai, M., Mochiduki, K., Yanagisawa, E., Sakashita, A.,
426 Wakai, T., Suzuki, Y., Ito, T., et al. (2013). High-resolution DNA methylome analysis of
427 primordial germ cells identifies gender-specific reprogramming in mice. *Genome Res.* *23*,
428 616–627.

429 Krueger, F., and Andrews, S.R. (2011). Bismark: a flexible aligner and methylation caller for
430 Bisulfite-Seq applications. *Bioinformatics* *27*, 1571–1572.

431 van de Lagemaat, L.N., Medstrand, P., and Mager, D.L. (2006). Multiple effects govern
432 endogenous retrovirus survival patterns in human gene introns. *Genome Biol.* 7, R86.

433 Lander, E.S., Linton, L.M., Birren, B., Nusbaum, C., Zody, M.C., Baldwin, J., Devon, K.,
434 Dewar, K., Doyle, M., FitzHugh, W., et al. (2001). Initial sequencing and analysis of the
435 human genome. *Nature* 409, 860–921.

436 Langmead, B., and Salzberg, S.L. (2012). Fast gapped-read alignment with Bowtie 2. *Nat.*
437 *Methods* 9, 357–359.

438 Lei, H., Oh, S.P., Okano, M., Juttermann, R., Goss, K.A., Jaenisch, R., and Li, E. (1996). De
439 novo DNA cytosine methyltransferase activities in mouse embryonic stem cells.
440 *Development* 122, 3195–3205.

441 Lerat, E., Rizzon, C., and Biémont, C. (2003). Sequence Divergence Within Transposable
442 Element Families in the *Drosophila melanogaster* Genome. *Genome Res.* 13, 1889–1896.

443 Maksakova, I.A., Romanish, M.T., Gagnier, L., Dunn, C.A., van de Lagemaat, L.N., and
444 Mager, D.L. (2006). Retroviral Elements and Their Hosts: Insertional Mutagenesis in the
445 Mouse Germ Line. *PLoS Genet* 2, e2.

446 Molaro, A., Falciatori, I., Hodges, E., Aravin, A.A., Marran, K., Rafii, S., McCombie, W.R.,
447 Smith, A.D., and Hannon, G.J. (2014). Two waves of de novo methylation during mouse
448 germ cell development. *Genes Dev.* 28, 1544–1549.

449 Murchison, E.P., Partridge, J.F., Tam, O.H., Cheloufi, S., and Hannon, G.J. (2005).
450 Characterization of Dicer-deficient murine embryonic stem cells. *Proc. Natl. Acad. Sci. U. S.*
451 *A.* 102, 12135–12140.

452 Ran, F.A., Hsu, P.D., Wright, J., Agarwala, V., Scott, D.A., and Zhang, F. (2013). Genome
453 engineering using the CRISPR-Cas9 system. *Nat. Protoc.* 8, 2281–2308.

454 Reik, W., and Surani, M.A. (2015). Germline and Pluripotent Stem Cells. *Cold Spring Harb.*
455 *Perspect. Biol.* 7.

456 Richardson, S.R., Gerdes, P., Gerhardt, D.J., Sanchez-Luque, F.J., Bodea, G.-O., Munoz-
457 Lopez, M., Jesuadian, J.S., Kempen, M.-J.H.C., Carreira, P.E., Jeddloh, J.A., et al. (2017).
458 Heritable L1 retrotransposition in the mouse primordial germline and early embryo. *Genome*
459 *Res.* gr.219022.116.

460 Robert, V.J.P., Sijen, T., Wolfswinkel, J. van, and Plasterk, R.H.A. (2005). Chromatin and
461 RNAi factors protect the *C. elegans* germline against repetitive sequences. *Genes Dev.* 19,
462 782–787.

463 Rowe, H.M., and Trono, D. (2011). Dynamic control of endogenous retroviruses during
464 development. *Virology* 411, 273–287.

465 Schorn, A.J., Gutbrod, M.J., LeBlanc, C., and Martienssen, R. (2017). LTR-Retrotransposon
466 Control by tRNA-Derived Small RNAs. *Cell* 170, 61–71.e11.

467 Seisenberger, S., Andrews, S., Krueger, F., Arand, J., Walter, J., Santos, F., Popp, C.,
468 Thienpont, B., Dean, W., and Reik, W. (2012). The Dynamics of Genome-wide DNA
469 Methylation Reprogramming in Mouse Primordial Germ Cells. *Mol. Cell* 48, 849–862.

470 Sharif, J., Endo, T.A., Nakayama, M., Karimi, M.M., Shimada, M., Katsuyama, K., Goyal, P.,
471 Brind'Amour, J., Sun, M.-A., Sun, Z., et al. (2016). Activation of Endogenous Retroviruses in

472 Dnmt1(-/-) ESC Involves Disruption of SETDB1-Mediated Repression by NP95 Binding to
473 Hemimethylated DNA. *Cell Stem Cell* 19, 81–94.

474 Stadler, M.B., Murr, R., Burger, L., Ivanek, R., Lienert, F., Schöler, A., Erik van Nimwegen,
475 Wirbelauer, C., Oakeley, E.J., Gaidatzis, D., et al. (2011). DNA-binding factors shape the
476 mouse methylome at distal regulatory regions. *Nature* 480, 490–495.

477 Svoboda, P., Stein, P., Anger, M., Bernstein, E., Hannon, G.J., and Schultz, R.M. (2004).
478 RNAi and expression of retrotransposons MuERV-L and IAP in preimplantation mouse
479 embryos. *Dev. Biol.* 269, 276–285.

480 Tam, O.H., Aravin, A.A., Stein, P., Girard, A., Murchison, E.P., Cheloufi, S., Hodges, E.,
481 Anger, M., Sachidanandam, R., Schultz, R.M., et al. (2008). Pseudogene-derived small
482 interfering RNAs regulate gene expression in mouse oocytes. *Nature* 453, 534–538.

483 Tang, W.W.C., Kobayashi, T., Irie, N., Dietmann, S., and Surani, M.A. (2016). Specification
484 and epigenetic programming of the human germ line. *Nat. Rev. Genet.* 17, 585–600.

485 Trapnell, C., Pachter, L., and Salzberg, S.L. (2009). TopHat: discovering splice junctions with
486 RNA-Seq. *Bioinformatics* 25, 1105–1111.

487 von Meyenn, F., Iurlaro, M., Habibi, E., Liu, N.Q., Salehzadeh-Yazdi, A., Santos, F., Petrini,
488 E., Milagre, I., Yu, M., Xie, Z., et al. (2016). Impairment of DNA Methylation Maintenance Is
489 the Main Cause of Global Demethylation in Naive Embryonic Stem Cells. *Mol. Cell* 62, 848–
490 861.

491 Walsh, C.P., Chaillet, J.R., and Bestor, T.H. (1998). Transcription of IAP endogenous
492 retroviruses is constrained by cytosine methylation. *Nat. Genet.* 20, 116–117.

493 Walter, M., Teissandier, A., Pérez-Palacios, R., and Bourc’his, D. (2016). An epigenetic
494 switch ensures transposon repression upon dynamic loss of DNA methylation in embryonic
495 stem cells. *eLife* 5, e11418.

496 Watanabe, T., Takeda, A., Tsukiyama, T., Mise, K., Okuno, T., Sasaki, H., Minami, N., and
497 Imai, H. (2006). Identification and characterization of two novel classes of small RNAs in the
498 mouse germline: retrotransposon-derived siRNAs in oocytes and germline small RNAs in
499 testes. *Genes Dev.* 20, 1732–1743.

500 Yang, N., and Kazazian, H.H. (2006). L1 retrotransposition is suppressed by endogenously
501 encoded small interfering RNAs in human cultured cells. *Nat. Struct. Mol. Biol.* 13, 763–771.

502 Yoshimizu, T., Sugiyama, N., De Felice, M., Yeom, Y.I., Ohbo, K., Masuko, K., Obinata, M.,
503 Abe, K., Schöler, H.R., and Matsui, Y. (1999). Germline-specific expression of the Oct-
504 4/green fluorescent protein (GFP) transgene in mice. *Dev. Growth Differ.* 41, 675–684.

505

506 **Figure Legends**

507 **Figure 1: Transcriptional upregulation of specific TE classes upon acute *Dnmt1* deletion**

508 (A) (left) Schematic overview of epigenetic reprogramming during preimplantation and male
509 (blue) and female (red) germline development. (right) Schematic of *Dnmt1* cKO as an *in vitro*
510 system for mechanistic study of TE regulation during epigenetic reprogramming.

511 (B) Violin plots showing the distribution of CpG methylation levels measured by WGBS-seq
512 of WT (grey) and conditional *Dnmt1* cKO ESC induced for days depicted in the figure. The
513 percentage of methylated cytosines was quantified in consecutive 50 CpG windows genome-
514 wide. CGI = CpG Island. For significance analysis Wilcoxon rank sum test with Bonferroni
515 correction testing with a p-value threshold of < 0.05.

516 (C) Heatmap of unbiased hierarchical clustering of all TEs responsive to *Dnmt1* cKO across
517 the time-course of KO induction. It shows relative expression (z-score) of TEs upon *Dnmt1*
518 cKO, n=2.

519 (D) Bar graph showing percentage of genic antisense transcription upon *Dnmt1* deletion in
520 KO relative to WT samples, n=2.

521 (E) Chromosome view of TE inserted antisense to gene. Position of TE is denoted (top
522 panel) along with sense strand specific RNA-seq reads (lower panels, sense transcription
523 shown in blue, antisense transcription shown in red). Each read is depicted. Arrows indicate
524 directionality of reads.

525 (F) Sense/Antisense expression of TEs as determined by RNA-seq analysis of conditional
526 *Dnmt1* cKO ESC uninduced (black), induced for days depicted in figure. Crosshatched bars
527 depict antisense reads. The figure shows mean of n=2.

528 See also Figure S2, S4I, Data S1.

529

530 **Figure 2: Small RNAs are being produced from TEs upon loss of *Dnmt1***

531 (A) Schematic displaying the hypothesis model of pervasive transcription overlapping TEs
532 acting as a trap of transcriptional activation of TEs. This could work through the production of
533 dsRNAs from sense and antisense transcripts that feed into the RNAi pathway which
534 subsequently silences the TEs.

535 (B) Small RNA-seq mapped to different classes of TEs of WT (grey) and conditional *Dnmt1*
536 cKO ESC induced for days depicted in figure. *p<0.05, ** p<0.005, two-tailed student t-test.
537 Bars represent mean +/- SD, n=3. All reads of a size between 20-24 nt have been mapped to
538 TE consensus sequence.

539 (C) Small RNA-seq mapped to consensus sequence of IAPEZ. All reads of a size between
540 20-36 nt have been mapped to the IAPEZ consensus sequence.

541 (D) Schematic displaying AGO2 IP of small RNAs.

542 (E) Size distribution of AGO2 bound small RNAs after AGO2 IP of sense (black) and
543 antisense (grey) small RNAs mapping to repeatmasker consensus sequences using the
544 piPipes small RNA-seq pipeline (Han et al., 2014).
545 (F) Small RNA-seq of AGO2 bound small RNAs mapped to TE classes of WT (grey) and
546 conditional *Dnmt1* cKO ESC induced for 9 days (light blue). *p<0.05, **p<0.005, two-tailed
547 student t-test. Bars represent mean +/- SD, n=4.
548 See also Figure S2, S4I, Data S1.

549

550 **Figure 3: TEs are repressed by a DICER mechanism**

551 (A) Knockdown (KD) of RNAi players (upper left) Schematic of siRNA KD in *Dnmt1* cKO
552 ESCs: the genome gets demethylated (orange), IAPs get transcriptionally activated and
553 resiliated (red) if small RNAs are present (grey), however KD of the RNAi pathway will
554 deplete small RNAs, (lower left) RT-qPCR analysis showing KD efficiencies of *Dicer*, *Ago2*
555 and *Dgcr8* upon treatment with siRNAs. (right) Expression of IAPs upon *Dicer*, *Ago2*, *Dgcr8*
556 or non-targeting siRNA transfection. The data is normalised to non-targeting control. Bars
557 represent mean +/- SD, n=3. *p<0.05, **p<0.005, two-tailed student t-test.

558 (B) Small RNA-seq of *Dicer/Dnmt1* cDKO and *Dnmt1* cKO ESCs. Sense (orange), antisense
559 (blue) small RNAs are separated by size and were mapped to all TEs. Reads were
560 normalised to non-induced WT (*Dicer*^{fl/fl} /*Dnmt1*^{fl/fl}) ESCs, n=1.

561 (C) RT-qPCR analysis of TE classes in ESCs following conditional *Dnmt1* cKO, *Dnmt1/Dicer*
562 cDKO by treatment with 4OHT or *Dicer* KO. Bars represent mean of 2 biological replicates
563 with 2 technical replicates. Values were normalized to *Atp5b*, *Hspcb* and major satellites
564 were normalised to U1. *p<0.05, **p<0.005, two-tailed student t-test.

565 (D) RT-qPCR analysis of IAPEz in the indicated ESC lines. Conditional deletions were
566 induced by treatment with 4OHT for the indicated days. Values were normalized to *Atp5b*
567 and *Hspcb* and are relative to the respective WT sample for each KO line, indicated by
568 dashed line. Error bars represent mean +/- SD, n=3 for *Dnmt1* cKO, *Dicer* KO/*Dnmt1* cKO
569 and *Ago2* KO/*Dnmt1* cKO and n=2 for *Dicer/Dnmt1* cDKO, *Ago2/Dnmt1* cDKO. *Ago2*
570 KO/*Dnmt1* cKO time points day 9 and 11 were not collected.

571 (E) Heatmap of unbiased hierarchical clustering of all TE classes responsive to *Dicer* KO.
572 Heatmaps depicts relative expression (z-score) of TEs upon *Dicer* KO, n=1.

573 See also Figure S4, S5, Table S2, S4I.

574

575 **Figure 4: Repressive Histone modifications enriched at TEs upon global demethylation**

576 (A) Heatmap showing relative enrichment (z-score) of repressive Histone marks (H3K9me3,
577 H3K27me3 and H3K9me2) at TE classes differentially regulated upon both *Dicer* KO (Figure
578 3A) and *Dnmt1* cKO (Figure 1C) and normalised to enrichment in WT ESCs.

579 (B) H3K27me3, H3K9me3 and H3K9me2 enrichment over TEs dependent on *Dicer* and
580 *Dnmt1*. Heatmap depicts ChIP-seq data of H3K27me3 mapped to TE families at depicted
581 days after *Dnmt1* cKO, *Dicer* KO and *Dnmt1/Dicer* cDKO in comparison to WT ESCs.

582 (C) Schematic of the two levels of TE control upon global demethylation. Upon deletion of
583 *Dnmt1*, DNA methylation (5mC; orange) mediated repression is lost, and transposon
584 expression increases (as an example IAP expression is shown in green). Subsequently small
585 RNAs (red; 'immediate' response) and repressive histone marks (chromatin, blue; 'chronic'
586 response) establish a new repressive environment. Also indicated are the time-points at
587 which the different experimental manipulations interfere with the system.

588 See also Figure S4, Data S1.

589

590 **Supplemental Information**

591 Supplemental Information includes Supplemental Experimental Procedures, four figures,
592 three tables and one data file.

593

594 **STAR Methods**

595 **CONTACT FOR REAGENT AND RESOURCE SHARING**

596 Further information and requests for resources and reagents should be directed to and will
597 be fulfilled by the Lead Contact, Rebecca Berrens (rebecca.berrens@gmail.com). The Ago2
598 antibody for was obtained from EMBL, after establishing an MTA with the laboratory of Prof.
599 Donal O'Carroll at University of Edinburgh.

600

601 **EXPERIMENTAL MODEL AND SUBJECT DETAILS**

602 **Cell lines**

603 Mouse embryonic stem cell (ESC) lines were used in this study. *Dnmt1*^{loxP/loxP} ESCs (strain
604 C57BL/6) were obtained from Haruhiko Koseki, RIKEN Center for Integrative Medical
605 Sciences, Yokohama City, Japan (Sharif et al., 2016). *Dicer/Dnmt1* cDKO, *Ago2/Dnmt1*
606 cDKO, *Dicer* KO and *Ago2* KO ESC lines were generated using *Dnmt1*^{loxP/loxP} ESCs using the
607 CRISPR/Cas9 targeting and screening primers mentioned in Table S3.

608

609 **Mice**

610 All *in vivo* PGC samples were collected from timed matings of C57Bl/6J female mice
611 carrying the Oct4-GFP transgene expressed in the developing gonad (Yoshimizu et al.,
612 1999). Primordial germ cells from male and female embryos at E13.5 and E14.5 were
613 collected. All procedures were covered by a project license (to WR) under the Animal
614 (Scientific Procedures) Act 1986, and is locally regulated by the Babraham Institute Animal
615 Welfare, Experimentation, and Ethics Committee.

616

617

618 **METHOD DETAILS**

619 **DNA/RNA Extraction**

620 Genomic DNA was prepared using QIAmp DNA Micro Kit (QIAGEN). RNA was extracted
621 using TriReagent (Sigma) and Phase Lock tubes (5Prime) following manufacturers'
622 instructions and subjected to DNase treatment using the DNA-free kit (Ambion DNA-free
623 DNA Cat #1311027) according to the manufacturers' instructions.

624

625 **Small RNA RT-qPCR**

626 For small RNA qPCR Taqman miRNA kits were used according to the manufacturer's'
627 instructions for mmu_miR93 (Taqman, Cat. No. TM001090), mmu_miR7081_mat (Taqman,
628 Cat. No. TM467052_mat) and snoRNA202 (Taqman, Cat. No. 001232) was used as a
629 positive control. RT-qPCR primers are listed in Table S2.

630

631 **AGO2 IP**

632 ESCs were cultured on 15 cm dishes and harvested in 1 x PBS. Pellets were frozen at -80°C
633 until further processing. ESC were resuspended in 300 µl Lysis buffer (50 mM Tris, pH8,
634 150 mM NaCl, 5 mM MgCl₂, 15 % Glycerol, 1 mM DTT, 0.5% Sodium deoxycholate,
635 0.5% Triton X-100, Protease inhibitor cocktail (Roche), 50µg/ml yeast tRNA, 2mM Vanadyl
636 ribonucleoside complex) and cells were pelleted at 10,000 rpm, 10 min, 4°C. The
637 supernatant was used as whole ESC extract. 25 µL beads (protein G Sepharose) were
638 washed 3 times with 1 mL of Wash Buffer (10 mM Tris pH 8, 150 mM NaCl, 1 mM MgCl₂,
639 0,01% NP-40). 50 µl of purified AGO2 antibody (O'Carroll lab) was added, filled up to 1mL
640 with Wash Buffer and incubated O/N at 4°C in a rotating wheel. On the next day, the beads
641 were washed 3 times with Wash Buffer and the negative control (beads with extract but
642 without serum) was prepared. The ESC extract was pre-spun to remove precipitated proteins
643 and 200µL extract was added to the beads and filled up to 600µL with Lysis buffer. The mix
644 was incubated for 2-4h at 4°C in a rotating wheel and subsequently washed 5 times with
645 wash buffer and the IP was eluted with 300µL Proteinase K buffer (10 mM Tris pH 7,5, 0,5%
646 SDS, 5 mM EDTA, 1 µL Proteinase K/reaction) after 30 min for 50°C incubation on the
647 thermomixer, at 850 rpm. RNA was isolated by phenol extraction and eluted in 8 µl H₂O.

648

649 **RNAi knockdown of Ago2, Dicer1, Dgcr8 in Dnmt1fl/fl ES cells**

650 RNA interference experiments were performed according to manufacturers' instructions with
651 modifications. Transfections of Dharmacon siGENOME SMARTpool siRNA against mouse
652 *Dicer* (Dharmacon, Cat. No. MU-040892-01-0005), *Dgcr8* (Dharmacon, Cat. No. MU-
653 051365-00-0002) or *Ago2* (Dharmacon, Cat. No. MU-058989-01-0005) and siGENOME non-
654 targeting siRNA#2 (Dharmacon, Cat. No. D-001210-02-05) were performed with
655 Lipofectamine 2000 according to the manufacturers' instructions. The transfection was done
656 in two rounds. The cells were plated at a density of 1 x 10⁵ ES cells per well of gelatinized
657 12-well plate. One day later the first transfection was done the following for each well of a 12
658 well plate: 50uM siRNA were added to 100 ul DMEM. 6 ul of Lipofectamin2000 were mixed
659 with 100 ul DMEM. The mix was incubated for 5 min at room temperature. Afterwards the
660 two solutions were mixed and incubated at room temperature for 15 min. 200 ul of the siRNA
661 and Lipofectamin2000 mix were added to each well of a 12 well plate. On the third day the
662 medium was changed. On the fourth day the second transfection was done the following:
663 125uM siRNA were added to 250 ul DMEM. 7.5 ul of Lipofectamin2000 were added to 250 ul
664 DMEM and incubated at room temperature for 5 min. The solutions were then mixed and
665 again incubated for 15 min at room temperature. The cells were washed with PBS,
666 trypsinised, inactivated and resuspended in ESC medium and plated on a gelatinised 6-well
667 plate I a total volume of 1.8 ml each well. 500ul of siRNA and Lipofectamin2000 were added

668 to each well. The ESCs were incubated at 37C for 6 hours and then the medium was
669 changed.

670 Cells were harvested 48 h after the 2nd transfection and RNA was extracted and analysed.

671

672 ***RT-qPCR***

673 100 ng -1 µg of DNase treated RNA was reverse transcribed (Thermo RevertAid #K1622)
674 using random hexamer primers. Endogenous controls (*Atp5b*, *Hspcb*, *U1*) were used to
675 normalise expression. Major satellite RT-qPCR was done as previously described (Lehnertz
676 et al., 2003, Probst et al., 2010). Primers are listed in Table S2.

677

678 ***CRISPR cKO and KO***

679 guideRNAs (gRNAs) were constructed following <https://chopchop.rc.fas.harvard.edu/> and
680 <http://crispr.mit.edu/> and cloned following the protocol by (Ran et al., 2013) into
681 pSpCas9(BB)-2A-GFP (Addgene plasmid ID: 48138) or pSpCas9(BB)-2A-hCD4, constructed
682 by replacing the GFP in the pSpCas9(BB)-2A-GFP with human CD4. Cells were cultured on
683 feeder plates and transfected with 1 µg gRNA and 100 ng donor DNA, where appropriate,
684 using Lipofectamine 2000 transfection reagent. Cells were sorted for GFP in single cell
685 colonies into 96 well plates using flow cytometry or CD4 expression plating on 10cm dishes
686 as single cell colonies. Colonies were screened by PCR using MyTaq (Bioline, BIO-25044)
687 and Sanger sequencing. See Figure S4A, S4D, S5A, S5D for knock out strategy and Table
688 S2 for gRNAs, screening primers and donor DNA sequence.

689

690 ***Fluorescence-activated cell sorting (FACS)***

691 Cells were trypsinised and resuspended in PBS + 1% FBS and analysed on a LSR Fortessa
692 Cell Analyzer (BD). Cells were gated for singlets and living cells were identified using the
693 level of DAPI incorporation and the level of GFP signal was recorded for each cell.

694

695 ***CD4 pull down***

696 Cells were trypsinised and resuspended in 70 µl 1 x PBS and stained with human CD4
697 Microbead antibody (Miltenyl Biotec, Cat. No. 130-045-101) according to manufacturers'
698 instructions. The CD4 positive cells were enriched using MACS columns. Negative cells were
699 collected from flow through. The cells were eluted in 500 µl 1 x PBS.

700

701 ***In vivo PGC collection***

702 All embryonic samples for library preparation were collected from timed matings of C57Bl/6J
703 female mice PGCs that express the Oct4-GFP transgene in the developing gonad
704 (Yoshimizu et al., 1999). E13.5 and E14.5 PGCs, male and female samples were collected

705 separately and after collagenase digestion PGC samples were sorted for GFP positive cells
706 using a FACSAria (BD) cell sorter with >98% purity.

707

708 ***Cell lines and culture conditions***

709 Mouse ESCs were cultured with or without feeders on gelatinized plates (0.1% gelatin) in
710 serum-containing media (DMEM 4,500 mg/l glucose, 4 mM L-glutamine, 15% fetal bovine
711 serum, 1 U/ml penicillin, 1 µg/ml streptomycin, 0.1 mM nonessential amino acids, 50 µM β-
712 mercaptoethanol) supplemented with mouse LIF at 37°C and 5% CO₂. Conditional deletion
713 was induced by Cre mediated recombination, as described before (Sharif et al., 2016). Cre
714 expression was induced in response to tamoxifen (4OHT, 800 nM).

715

716 ***WGBS-seq libraries***

717 For preparation of WGBS-seq libraries, genomic DNA was sonicated using a Covaris
718 Sonicator, followed by end-repair, A-tailing and methylated adapter (Illumina) ligation using
719 NEBNext reagents (E6040S, NEB). Afterwards the libraries were bisulfite treated using
720 Imprint DNA modification kit (MOD50-1KT, Sigma), followed by library amplification with
721 indexed primers using KAPA HiFi Uracil HotStart DNA Polymerase (KAPA HiFi Uracil+,
722 KK2801/2). Subsequently, the amplified libraries were purified and assessed for quality and
723 quantity using High-Sensitivity DNA chips on an Agilent Bioanalyzer. High-throughput
724 sequencing of all libraries was carried out with a 75 bp or 50 bp paired-end (PE) sequencing
725 on Illumina HiSeq 2500 instruments using TruSeq reagents (Illumina, San Diego, CA, USA),
726 according to manufacturers' instructions.

727

728 ***ChIP-seq libraries***

729 ESCs were grown on 15 cm dishes coated with 0.1 % gelatine until they were 80 %
730 confluent. Subsequently cells were cross-linked with 1 % methanol-free formaldehyde in
731 fresh medium for 10 minutes. To quench the cross-linking, 0.2 M final concentration of
732 glycine was added. ESCs were washed twice with ice cold 1 x PBS (137 mM NaCl, 2.7 mM
733 KCl, 10 mM Na₂HPO₄, 2 mM KH₂PO₄ dissolved in 800 ml distilled H₂O, pH was adjusted to
734 7.4 with HCl) and harvested using a cell scraper. Cells were then pelleted by centrifugation at
735 8,000 x g at 4 °C for 3 min. Pellets were resuspended in LB1 bu er (50 mM HEPES' KOH, pH
736 7.5; 140 mM NaCl; 1 mM EDTA; 10 % glycerol; 0.5 % NP-40; 0.25 % Triton X-100, protease
737 inhibitors) for 10 minutes at 4°C, pelleted and resuspended in LB2 buffer (10 mM Tris/HCl,
738 pH 8.0; 200 mM NaCl; 1 mM EDTA; 0.5 mM EGTA, protease inhibitors) for 10 minutes at 4
739 °C. Cells were pelleted and resuspended in LB3 bu er (10 mM Tris-HCl, pH 8; 100 mM NaCl;
740 1 mM EDTA; 0.5 mM EGTA; 0.1% Na/Deoxycholate; 0.5% N-Lauroylsarcosine, protease
741 inhibitors). Next the cells were sonicated using Misonix Sonicator 3000. Triton X-100 was

742 added to a final concentration of 1 % and the lysate was centrifuged at 20,000 x g for 10 min
743 to pellet the debris. The bead-antibody complexes were prepared before adding the
744 sonicated DNA. Protein G-coupled Dynabeads (Thermo Fisher Scientific, Cat. No. 10003D)
745 and the primary antibodies in PBS with 5 mg/ml BSA were incubated ON. Subsequently, the
746 bead-antibody complexes were added to the sonicated chromatin and both were incubated
747 at 4 °C ON. On the following day, beads were washed extensively with RIPA buffer (50 mM
748 HEPES pH 7.6, 1 mM EDTA, 0.7 % Na deoxycholate, 1 % NP-40, 0.5M LiCl), once with 1x
749 TE bu er (1 M Tris-HCl (pH approximately 8.0), 0.1 M EDTA) and eluted in 200 µl of buffer
750 containing 1 % SDS and 0.1 M NaHCO₃. They were then incubated at 65°C ON for reverse
751 cross-linking. RNase A treatment at 37°C was carried out for 1 h, then Proteinase K
752 treatment at 55°C for 2 h. The DNA was then extracted with phenol/chloroform, followed by
753 ethanol precipitation. ChIP-seq library preparation was performed using MicroPlex Library
754 Preparation kit (Diagenode) following manufacturer's instructions. Libraries were quantified
755 using the High Sensitivity DNA Bioanalyzer kit and Kapa library quantification. High-
756 throughput sequencing of all libraries was carried out with a 100 bp PE sequencing on
757 Illumina HiSeq 2500 instruments.

758

759 ***Small RNA-seq libraries***

760 Small RNA-seq libraries were produced according to the Illumina protocol (RS-200-0012),
761 with the following changes: 10 ng or 1 µg RNA (RIN of 8-10) were used as input material.
762 The instructions were followed until the cDNA purification. In order to purify the cDNA, the
763 samples were run on 10 % Novex PAGE gel. The entire area between the 145 and 160 bp
764 markers was excised, gel purified by addition of 0.3 M NaCl and the DNA was eluted from
765 the gel by rotation over night at 4°C. The DNA was precipitated in EtOH overnight and the
766 library was quantified using the HighSensitivity Bioanalyzer kit. The small RNA-seq libraries
767 were additionally quantified by Kapa Library Quantification. The libraries were pooled
768 according to their molecular weight. High-throughput sequencing of all libraries was carried
769 out with a 50 bp SE on Miseq or SE and PE on Illumina HiSeq 2500 instruments.

770

771 ***Total RNA-seq libraries***

772 Stranded Total RNAseq libraries were prepared according to manufacturers' protocols using
773 the Illumina stranded Total RNAseq library preparation after Ribo-zero depletion. High-
774 throughput sequencing of all libraries was carried out with a 100 bp PE on Illumina HiSeq
775 2500 instruments.

776

777

778 **QUANTIFICATION AND STATISTICAL ANALYSIS**

779 ***WGBS-seq mapping and analysis***

780 Raw sequence reads from WGBS libraries were trimmed to remove poor quality reads and
781 adapter contamination, using Trim Galore (v0.4.1,
782 http://www.bioinformatics.babraham.ac.uk/projects/trim_galore/) with default parameters. The
783 remaining sequences were mapped using Bismark (v0.14.4) (Krueger and Andrews, 2011)
784 with default parameters to the mouse reference genome Ensembl v67 NCBIM37 in paired-
785 end mode. Reads were then deduplicated and CpG methylation calls were extracted from
786 the deduplicated mapping output using the Bismark methylation extractor (v0.14.4) in paired
787 end mode. CpG methylation calls were analysed using R and SeqMonk software
788 (www.bioinformatics.babraham.ac.uk/projects/seqmonk/). The custom R scripts can be found
789 in Data S1. Global CpG methylation levels of pooled replicates were calculated in windows of
790 50 CpGs with a coverage of at least 3, illustrated using bean plots. Methylation over a given
791 genomic feature was calculated by averaging the individual methylation levels of CpGs
792 covered by at least 3 reads and only features with at least 50 CpGs were used. Promoters
793 were defined as the region -1 kb to the transcription start site as annotated in Ensembl
794 NCBIM37 v67. For analysis of specific genome features these were defined as follows: Gene
795 bodies (probes overlapping genes), CGI promoters (promoters containing a CGI) (Illingworth
796 and Bird, 2009), non-CGI promoters (all other promoters).

797

798 ***RNA-seq mapping and analysis***

799 RNA-seq sequences were trimmed using Trim Galore using default settings. Trimmed
800 sequencing reads were aligned to mouse genome assembly NCBIM37 using TopHat
801 (Trapnell et al., 2009) and reads with MAPQ scores <20 were discarded. Mapped RNA-seq
802 data were quantitated using the RNA-seq quantitation pipeline in SeqMonk software to
803 generate log₂ RPM (reads per million reads of library) expression values. Genes were
804 considered to be differentially expressed if they were significantly different ($p < 0.05$ after
805 Benjamini and Hochberg multiple testing correction) when analysed with both DESeq2 and
806 Intensity difference (SeqMonk) statistical tests.

807

808 Global pervasive transcription, was calculated as following: Genes with significant antisense
809 expression were identified by initially counting both sense and antisense reads over all genes
810 in the genome. A global expected antisense level was defined by the total proportion of
811 antisense reads across all genes. Individual genes were considered to show significant
812 antisense expression if they had a binomial p-value <0.05 following multiple testing
813 correction (FDR) using the global antisense proportion as the expected success rate, the
814 total reads for that gene as the trials and the total antisense reads for that gene as
815 successes. Additionally, the raw antisense transcription counts for all samples was

816 calculated and significant differential antisense expression was calculated using DESeq2
817 with an FDR < 0.05. The overlap of the two quantifications was used to define pervasive
818 transcription, and the difference in antisense transcription between WT and KO samples at
819 each time point was plotted using R.

820

821 ***ChIP-seq mapping and analysis***

822 ChIP-seq sequencing data was trimmed to remove poor quality reads, adaptor and barcodes
823 sequences using Trim Galore. Trimmed data were mapped using Bowtie2 (Langmead and
824 Salzberg, 2012) against the mouse reference genome Ensembl v67 NCBIM37 and reads
825 with a MAPQ value < 20 were discarded. Mapped ChIP-seq data were quantitated creating
826 1kb tiles of the whole genome and calculating the log2 observed/expected value comparing
827 the observed read count with the expected count had all reads been uniformly distributed
828 over the genome.

829

830 ***Small RNA-seq mapping and analysis***

831 For small RNA-seq data analysis trimmed sequencing reads were filtered to 20-24nt length
832 and mapped to the mouse NCBIM37 genome assembly using Bowtie2. Raw overlap counts
833 for each small RNA molecule were quantitated using SeqMonk. Graphing and statistics was
834 performed using Excel or R. For consensus sequence mapping the piPipes small RNA
835 pipeline was used (<https://github.com/bowhan/piPipes>) (Han et al., 2015). IAPEZ consensus
836 sequences were used from repeatmasker libraries (repeatmasker v4.0.3, library version
837 20130422). Additionally, the small RNA-seq data processing was performed using the freely
838 available piRNA pipeline piPipes. For repeat mapping, trimmed data were mapped using
839 Bowtie2 against repeats as defined in the analysis by using the mouse repeatmasker
840 annotation. The plots shown were generated as described below: The distribution of small
841 RNAs was computed by mapping all small RNA-seq reads to the individual genomic
842 features. The length distribution was calculated taking all uniquely mapped small RNAs into
843 account, excluding small RNA-seq mapping to ribosomal RNAs (rRNAs). For all subsequent
844 analysis, small RNA reads were pre-filtered as follows: reads mapping to rRNAs and
845 miRNAs were excluded, then reads aligning to the repeat masked mm9 genome (all
846 annotated repeats were masked/replaced by Ns) were removed, too. The remaining small
847 RNAs reads were mapped to the mouse repeatmasker annotation. The 5' end nucleotide
848 composition was computed from the uniquely mapped small RNAs. Similarly, analysis of the
849 position of 5' to 5' overlap was performed on the mapped small RNAs reads and the length
850 distribution and strand orientation of small RNAs shown was generated using uniquely
851 mapped small RNA reads.

852

853 ***Transposon analysis***

854 Repeat locations for a pre-defined set of repeat classes of interest were extracted from the
855 pre-masked repeatmasker 4.0.3-20130422 library in the mm9 genome. Repeat instances
856 within 2 kb of an annotated gene in the Ensembl v67 NCBIM37 gene set were removed to
857 avoid mixing signals from genic expression with specific expression of repetitive sequences.
858 RNA-seq data were processed and mapped as described above (RNA-Sequencing Mapping
859 and Analysis). We set a standard outlier filtering approach with a cutoff of counts > 3.
860 Overlaps were quantitated between the mapped RNA-seq reads and the repeat instances.
861 This allowed an unbiased identification of TEs depending on *Dnmt1 KO* as well as *Dicer KO*,
862 which we followed throughout this manuscript. Summed counts for all instances of each
863 class of repeat were calculated and these were corrected for both the total length of all TEs
864 and the size of the individual libraries to generate log₂ RPM expression values. The matrix of
865 expression values and samples were plotted using the R pheatmap library allowing the
866 repeat classes to cluster using default parameters. WGBS-seq libraries were processed and
867 mapped as described below (Bisulfite Sequencing Mapping and Analysis). Methylation levels
868 at the repeat instances were quantitated by summing up all methylation calls and non-
869 methylation calls for all instances of each class of repeat and calculating the percentage of
870 methylated Cs over all Cs. Only TEs with at least 1000 observations in all samples were
871 used for the analysis and calculation of percentage methylation. For major satellite
872 methylation analysis Bismark (Krueger and Andrews, 2011) was used to map all reads
873 against the mouse major satellite consensus sequence (GSAT from repeatmasker) and the
874 methylation calls from these results were analyzed directly. The custom R scripts can be
875 found in Data S1.

876

877 **Statistics**

878 Statistical values including the exact number of replicates (n), the definition of standard
879 deviation and statistical significance are reported in the Figure Legends.

880 (1) WGBS-seq

881 For statistical analysis WGBS-seq of Figure 1A and S1 of WT versus *Dnmt1 KO* data we
882 used the Wilcoxon rank sum test with Bonferroni correction testing with a p-value threshold
883 of <0.05. The code of the analysis of the retained methylation over TEs can be found in Data
884 S1.

885 *(2) Total RNA-seq*

886 To call differentially expressed mRNAs, we applied the SeqMonk intensity difference filter
887 with Benjamini and Hochberg correction for multiple testing with a p-value threshold of <0.05
888 and overlapped them with the genes called differentially expressed by DESeq2 with a p-
889 value threshold of <0.05 and multiple testing correction.

890 For TE analysis we only considered significantly differentially expressed TEs p<0.05 of
891 Dnmt1 KO over WT samples into account. The code of the analysis can be found in Data S1.

892 *(3) small RNA-seq*

893 To call differentially expressed miRNAs we overlapped the differentially expressed miRNAs
894 using DESeq2 with multiple testing correction and SeqMonk intensity difference filter with
895 Benjamini and Hochberg correction with a p-value of <0.05.

896 To call differential amount of mapped small RNAs to TEs we used Students t-test to compare
897 day 8 to day 0 enrichment of small RNAs with a p-value of <0.05.

898 *(4) ChIP-seq*

899 As we only have data from one measurement we could not call significant differences of
900 histone modification enrichment but show TEs which have at least 2 times higher enrichment
901 in Dnmt1 KO versus WT samples. The code of the analysis can be found in Data S1.

902 *(5) RT-qPCR*

903 Each RT-qPCR was done with 3 technical replicates. Differences between conditions that
904 are statistically significant are denoted by *p-value<0.05, **p-value<0.005 using the standard
905 distributed two tailed t-test.

906 *(6) siRNA knock-down*

907 Every siRNA knock-down was done in 3 technical replicates. Differences between conditions
908 that are statistically significant are denoted by *p-value<0.05, ** p-value<0.005 using the
909 standard distributed two tailed t-test.

910

911 **DATA AND SOFTWARE AVAILABILITY**

912 The accession numbers for the next-generation-sequencing data reported in this study are
913 GEO: GSE89698. The software of this study can be found in Data S1.

914

KEY RESOURCES TABLE

REAGENT or RESOURCE	SOURCE	IDENTIFIER
Antibodies		
anti-CD4 microbead	Miltenyl Biotec	Cat #: 130-045-101
Alexa Fluor 647, goat anti-mouse IgG antibody	Thermo Fisher Scientific	Cat# A-21236 RRID:AB_141725
Alexa Fluor 568 donkey anti - rabbit IgG antibody	Thermo Fisher Scientific	Cat# A10042 RRID:AB_2534017
Rabbit Anti-Nanog Polyclonal Antibody, Unconjugated	Abcam	Cat# ab80892 RRID:AB_2150114
AGO2 antibody	Dr. O'Carrolls lab	
Histone H3K9me3 antibody	Active Motif	Cat #: 61013, RRID: AB_2687870
H3K27me3-mouse antibody	Active Motif	Cat #: 39155, RRID:AB_2561020
Histone H3K9me2 antibody	Abcam	Cat #: ab1220, RRID:AB_449854
Bacterial and Virus Strains		
E.coli: One Shot™ TOP10 chemically competent cells	Thermo Fisher Scientific	Cat #: K450001
Chemicals, Peptides, and Recombinant Proteins		
Tamoxifen	Sigma-Aldrich Co. Ltd	Cat #: T5648-1G
mouse LIF	Stem Cell Institute, Cambridge	N/A
Na/Deoxycholate	Sigma-Aldrich Co. Ltd	Cat #: D6750-10G
N-lauroylsarcosine	Sigma-Aldrich Co. Ltd	Cat #: 61739-5G
Vanadyl ribonucleoside complex	New England Biolabs	Cat #: S1402S
Lipofectamine 2000	Thermo Fisher Scientific	Cat #: 11668027
Protein G-coupled Dynabeads	Thermo Fisher Scientific	Cat #: 10003D
HiFi Uracil+ ReadyMix	KAPABiosystems	Cat #: KK2801
T4 RNA Ligase 2, truncated	New England Biolabs	Cat #: M0242S
Tri-Reagent	Sigma-Aldrich Co. Ltd	Cat #: T9424-200ML
Phenol/chloroform/isoamylalcohol (25:24:1)	Life Technologies Ltd	Cat #: 15593031
TritonX 100	Sigma-Aldrich Co. Ltd	Cat #: RES9690T
Dimethylsulfoxide (DMSO)	Thermo Fisher Scientific	Cat #: TS-20684
Ampicillin	Sigma-Aldrich Co. Ltd	Cat #: A9518-5G
Penicillin/Streptomycin	Thermo Fisher Scientific	Cat #: 15140122
L-glutamine	Thermo Fisher Scientific	Cat #: 25030081
Non-essential amino acids	Thermo Fisher Scientific	Cat #: 11140050
2-Mercaptoethanol (50mM)	Life technologies	Cat #: 31350-010
RNase A	Thermo Fisher Scientific	Cat #: EN0531
cOmplete™ Protease Inhibitor Cocktail	Sigma-Aldrich Co. Ltd	Cat #: 00000001169 7498001
Proteinase K	Thermo Fisher Scientific	Cat #: EO0491
Paraformaldehyde 16% Solution	Agar Scientific	Cat #: AGR1026
Gelatine	Sigma-Aldrich Co. Ltd	Cat #: G9391
DTT	Sigma-Aldrich Co. Ltd	Cat #: D0632-1G
Fetal Bovine Serum (FBS)	Stem Cell Institute, Cambridge	N/A

DMEM (High Glucose) w/L-Glutamine andamp; Na Pyr	Life technologies	Cat #: 41966-052
NEBuffer 2	New England Biolabs	Cat #: B7002S
Trypsin EDTA (1x) 100ml	Life technologies	Cat #: 25300-054
HyperLadder™ 1kb, 100bp	Bioline	Cat #: BIO-33053, BIO-33029
SYBR Safe	Invitrogen	Cat #: S33102
SYBR Gold	Life Technologies Ltd.	Cat #: S11494
PvuI	New England Biolabs	Cat #: R0150S
EcoRI HF	New England Biolabs	Cat #: R3101L
T4 Polynucleotide Kinase	New England Biolabs	Cat #: M0201L
T4 Ligase	New England Biolabs	Cat #: M0202T
Ampure XP beads	Beckman Coulter	Cat #: A63880
T5 Exonuclease	New England Biolabs	Cat #: M0363S
Exonuclease I	New England Biolabs	Cat #: M0293S
Klenow exo-	New England Biolabs	Cat #: M0212L
Glycoblu	Ambion	Cat #: AM9516
Optimem	Gibco	Cat #: 31985062
DAPI	Thermo Fisher Scientific	Cat #: 62248
MyTaq Redmix	Bioline	Cat #: BIO-25043
Orange G dye	Sigma-Aldrich Co. Ltd	Cat #: 861286-25G
Critical Commercial Assays		
TruSeq Small RNA Library Prep Kit -Set A (24 rxns) (Set A-c: indexes 1-36)	Illumina	Cat #:RS-200-0012, RS-200-0024, RS- 200-0036
NEBNext® DNA Library Prep Master Mix Set for Illumina®	New England Biolabs	Cat #: E6040S
Imprint ® DNA Modification Kit	Sigma-Aldrich Co. Ltd	Cat #: MOD50-1KT
TruSeq RNA library preparation kit v2	Illumina	Cat #: RS-122-2001
MicroPlex Library Preparation kit	Diagenode	Cat #: C05010012
SmallRNA qRT-PCR miRNA kit: mmu_miR93	Taqman	Cat #: TM001090
SmallRNA qRT-PCR miRNA kit: mmu_miR7081_mat	Taqman	Cat #: TM467052_mat
SmallRNA qRT-PCR miRNA kit: snoRNA202	Taqman	Cat #: 001232
Dharmacon siGENOME SMARTpool, mouse Dicer	Dharmacon	Cat #: MU-040892- 01-0005
Dharmacon siGENOME SMARTpool, mouse Dgcr8	Dharmacon	Cat #: MU-051365- 00-0002
Dharmacon siGENOME SMARTpool, mouse Ago2	Dharmacon	Cat #: MU-058989- 01-0005
Dharmacon siGENOME SMARTpool, mouse Dicer	Dharmacon	Cat #: D-001210-02- 05
Miniprep kit	Qiagen	Cat #: 27106
Gel extraction kit	GeneJET	Cat #: K0691
PCR Purification kit	GeneJET	Cat #: K0701
Qiaamp DNA micro kit	Qiagen	Cat #: 56304
TURBO DNA-free kit	Life Technologies Ltd	Cat #: AM1907
Quant-iT PicoGreen® dsDNA Assay kit	Life Technologies Ltd	Cat #: P11496
Platinum SYBR Green qPCR SuperMix-UDG w/ROX	Life Technologies Ltd	Cat #: 11744100
QuickExtract	Epicentre	Cat #: QE09050
Kapa Library Quantification kit	Kapa Biosystems	Cat #: KK4847

High Sensitivity DNA kit	Agilent	Cat #: 5067-4626
High Sensitivity total RNA kit	Agilent	Cat #: 5067-1513
Deposited Data		
Raw and analyzed data	This study	GEO: GSE89698
Mouse reference genome NCBI build 37, NCBIM37	Mouse Genome Sequencing Consortium	http://may2012.archive.ensembl.org/Mus_musculus/Info/Index
Mouse repeats	repeatmasker v4.0.3, library version 20130422	http://www.repeatmasker.org/
Mouse ESCs enhancer annotation track	Chen et al., 2012, Creighton et al., 2010	
CpG island promoters	Illingworth and Bird, 2009	
Promoters: regions -1kb to the transcription start site	Ensemble, NCBIM37 version 67	
Experimental Models: Cell Lines		
<i>Dnmt1</i> cKO: Passage 12 <i>Dnmt1</i> ^{loxP/loxP} (C57BL/6) ESCs	Sharif et al., 2016	N/A
<i>Dicer/Dnmt1</i> cDKO: Passage 21 <i>Dicer</i> ^{loxP/loxP} / <i>Dnmt1</i> ^{loxP/loxP} ESCs	This study	See STAR methods for details
<i>Ago2/Dnmt1</i> cDKO: Passage 21 <i>Ago2</i> ^{loxP/loxP} / <i>Dnmt1</i> ^{loxP/loxP} ES cells	This study	See STAR methods for details
<i>Dicer</i> KO: Passage 17 <i>Dicer</i> KO/ <i>Dnmt1</i> ^{loxP/loxP} ES cells	This study	See STAR methods for details
<i>Ago2</i> KO: Passage 17 <i>Ago2</i> KO/ <i>Dnmt1</i> ^{loxP/loxP} ES cells	This study	See STAR methods for details
Experimental Models: Organisms/Strains		
Mouse: C57Bl/6J female mice carrying the Oct4-GFP transgene in the developing gonad: B6.Cg-Tg(GOF18/EGFP)11Ymat/Rbrc	Yoshimizu et al., 1999	RRID:IMSR_RBRC00868
Oligonucleotides		
Primers for CRISPR clone generation, see Table S3	This paper	N/A
Primers for RTqPCR clone generation, see Table S2	This paper	N/A
Recombinant DNA		
Cas9 plasmid: pSpCas9(BB)-2A-GFP	Ran et al., 2013	Addgene Plasmid #48138
pSpCas9(BB)-2A-hCD4	This study	N/A
Software and Algorithms		
Bowtie2	Langmead and Salzberg, 2012	http://bowtie-bio.sourceforge.net/bowtie2/index.shtml
Bismark	Krueger and Andrews, 2011	https://www.bioinformatics.babraham.ac.uk/projects/bismark/ , version 0.14.4
TopHat	Trapnell et al., 2009	http://ccb.jhu.edu/software/tophat/index.shtml
piPipes	Han et al., 2015	https://github.com/bowhan/piPipes/wiki

Trim Galore	N/A	http://www.bioinformatics.babraham.ac.uk/projects/trim_galore/ , Version 0.4.1
SeqMonk software	N/A	www.bioinformatics.babraham.ac.uk/projects/seqmonk/
DESeq2	Love et al., 2014	https://bioconductor.org/packages/release/bioc/html/DESeq2.html , version 3.5
Transposon analysis	this study	supplement
R	Data analysis	https://www.r-project.org/ , version 3.2.5
Adobe Illustrator	Figures	http://www.adobe.com/de/products/illustrator.html , version CC 2015.3
Other		

Figure 1

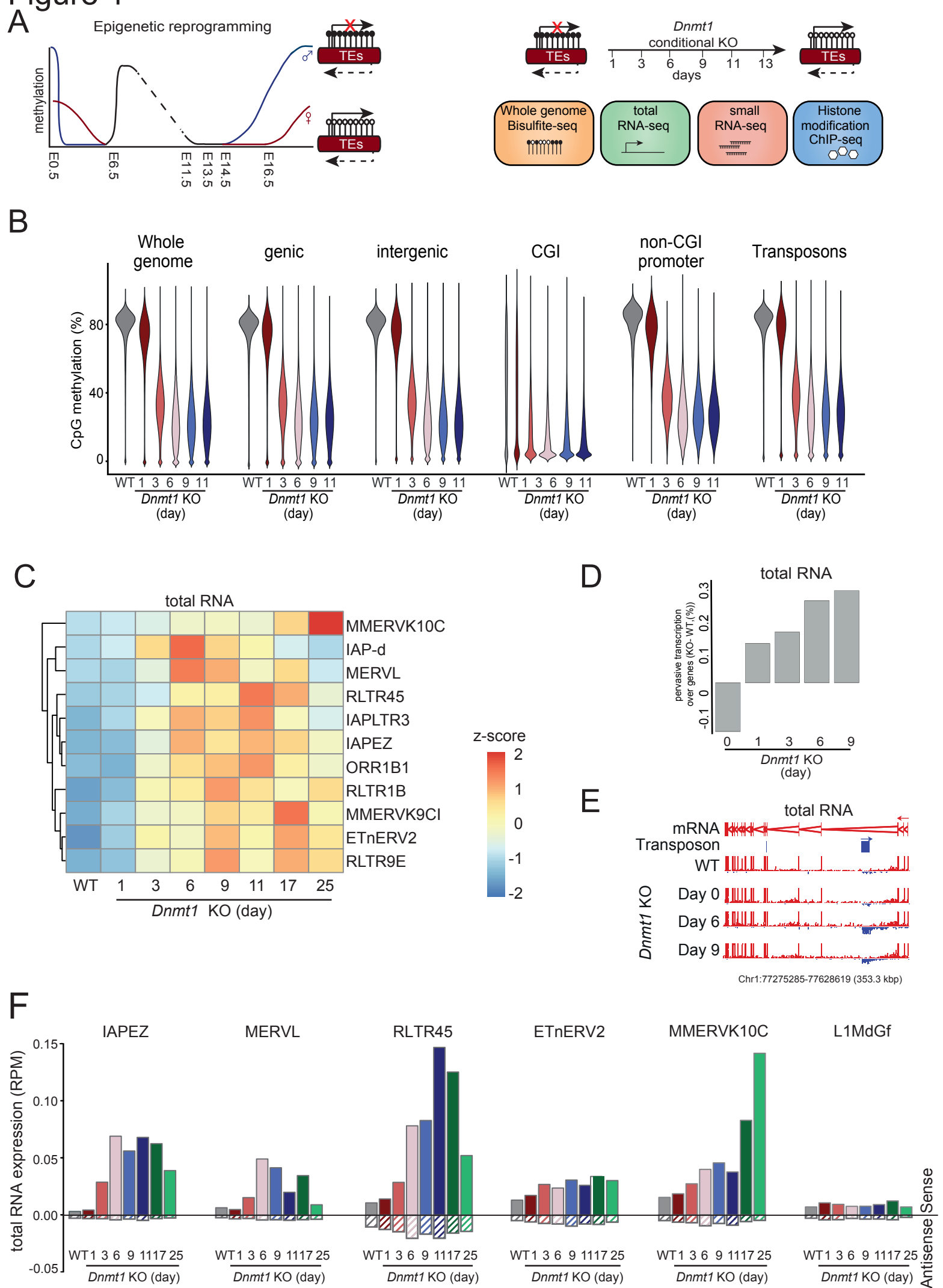
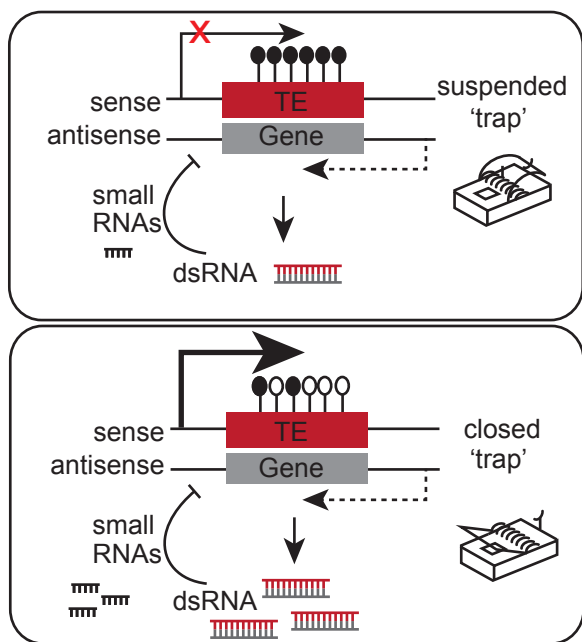
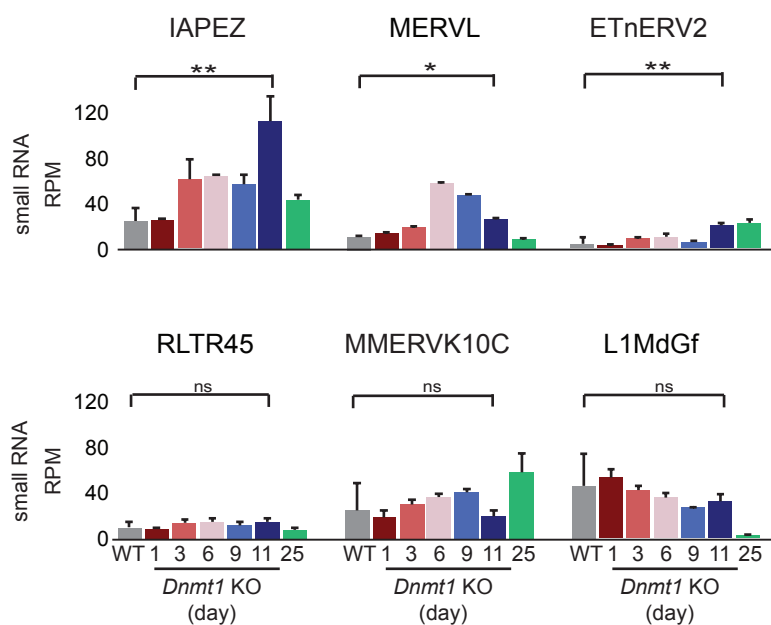


Figure 2

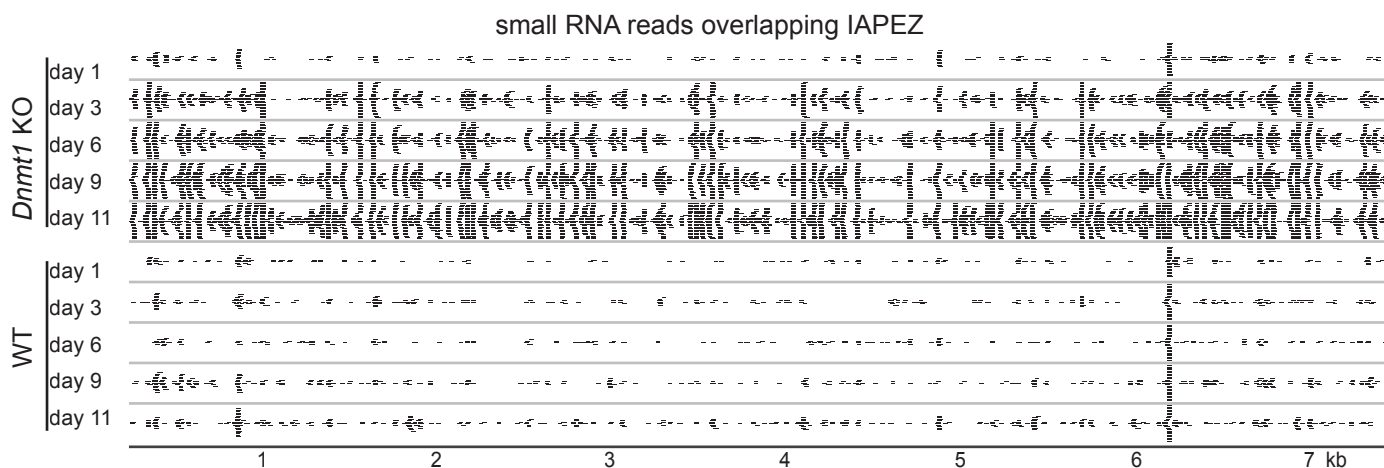
A



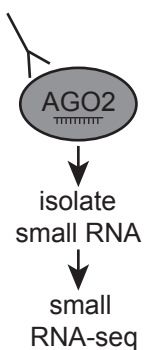
B



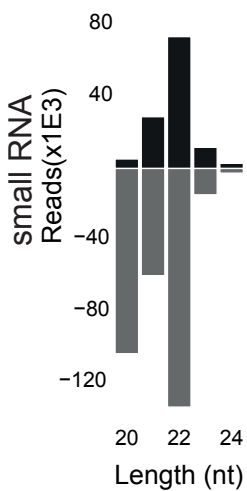
C



D



E



F

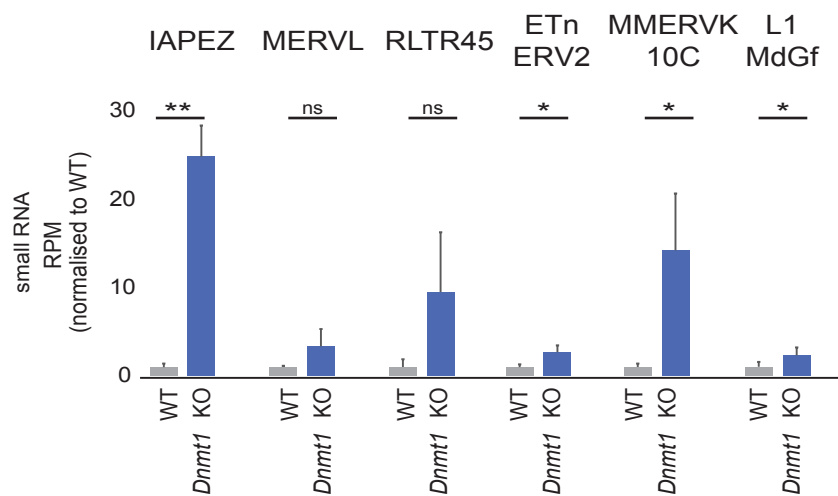
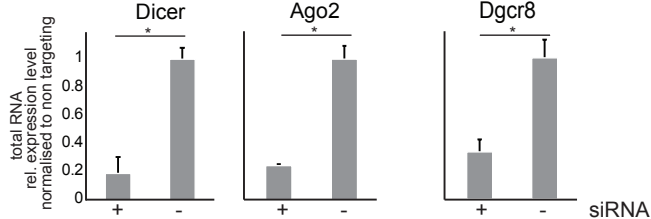
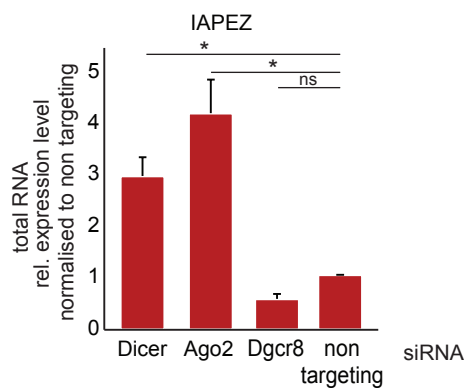
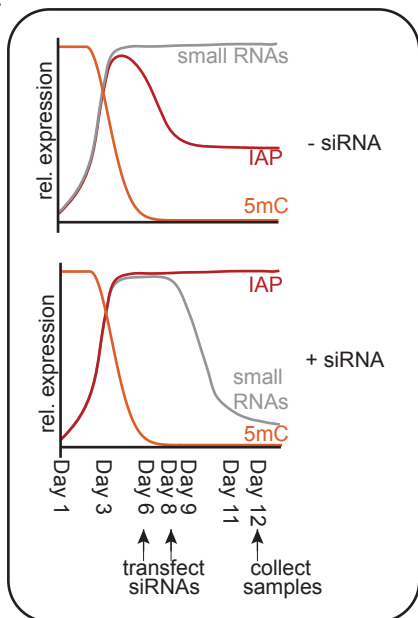
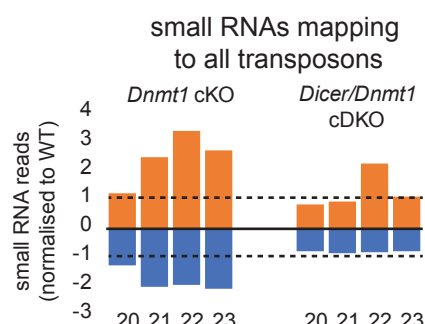


Figure 3

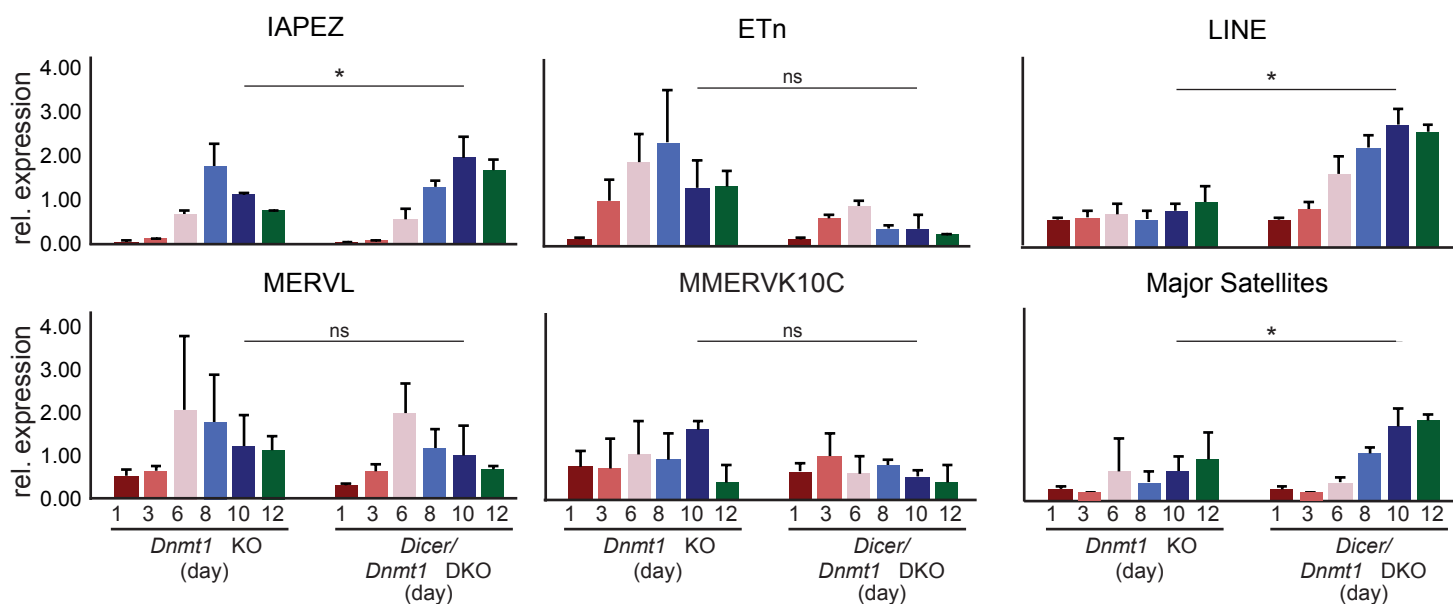
A



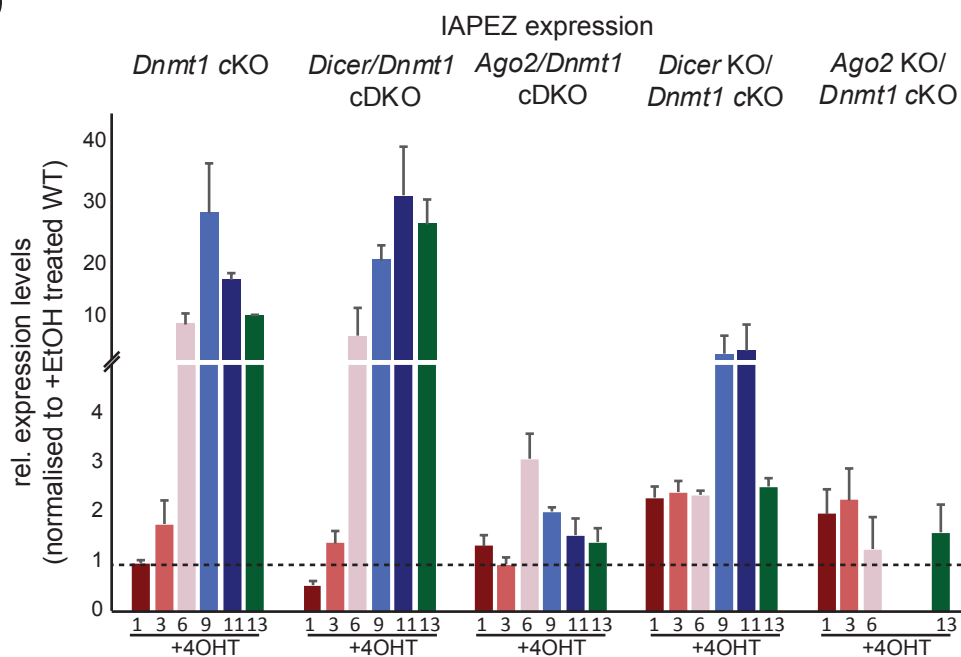
B



C



D



E

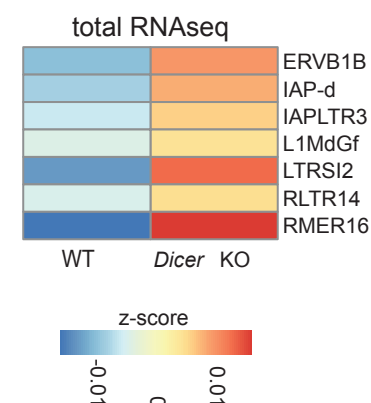
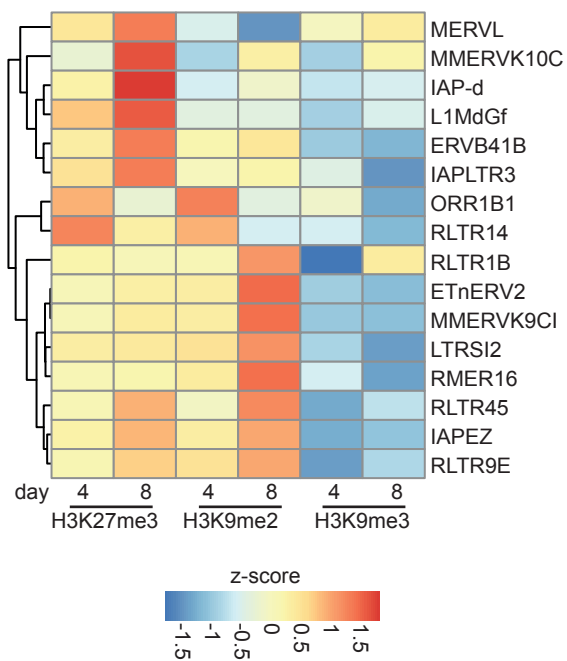
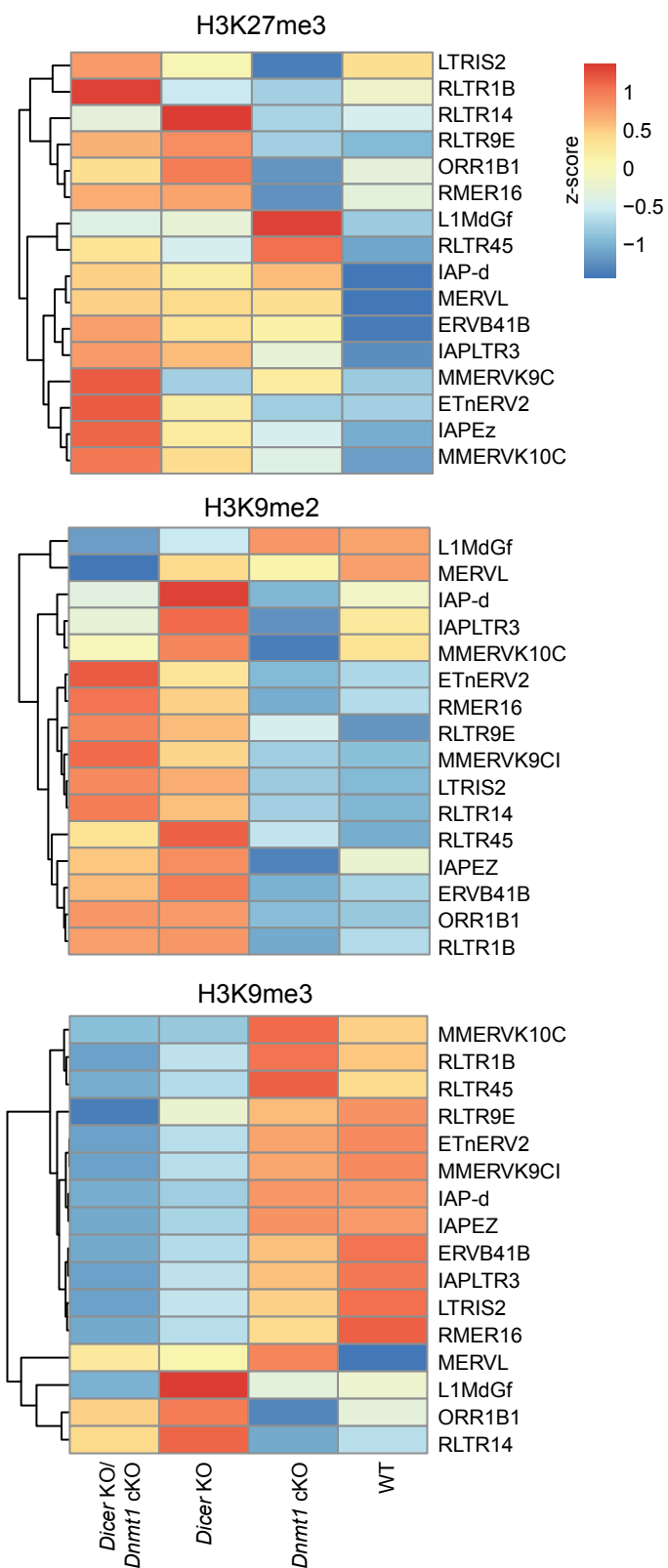


Figure 4

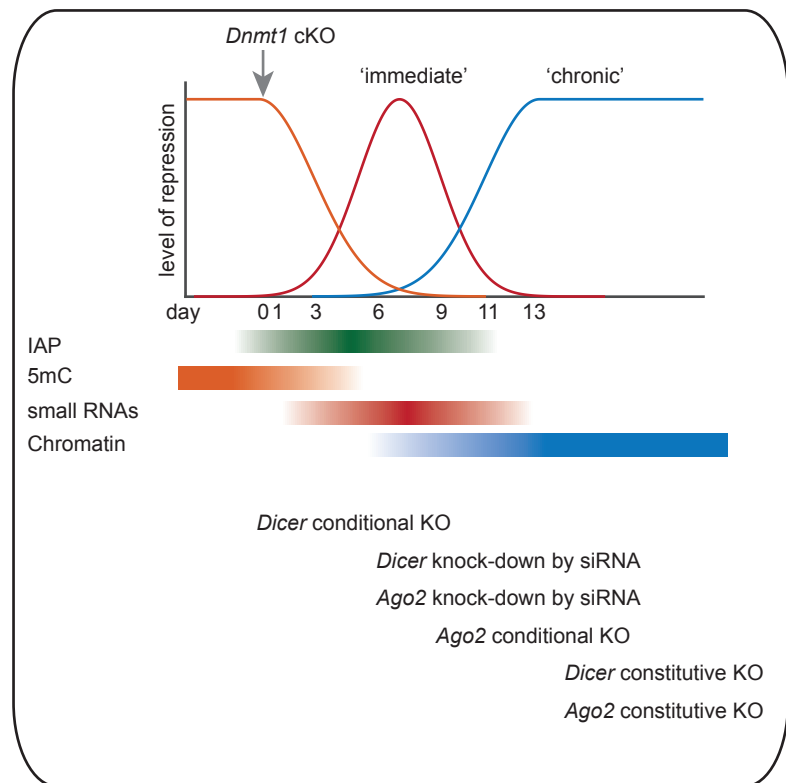
A



B



C



1 Supplemental Information

2

3 Supplemental Figure Legends

4 **Figure S1. Global DNA demethylation and transcriptional change upon acute *Dnmt1* deletion,**
5 **Related to Figure 1**

6 (A) WGBS-seq reads overlapping the whole Chromosome 2 between WT (day 1-day 11) and
7 *Dnmt1* cKO ESCs induced for 1-11 days. Percentage of methylated cytosines were counted
8 for each consecutive 50 CpG window genome-wide.

9 (B) Enrichment of CpG methylation over transcription starts sites (TSS) and gene body in WT
10 and *Dnmt1* cKO ESCs induced 1 day (dark red), 3 days (light red), 6 days (light pink), 9 days
11 (light blue), 11 days (dark blue). Measurement of 2 biological replicates. Percentage of
12 methylated cytosines were counted for each consecutive 50 CpG window genome-wide.

13 (C) Bean plots showing distribution of methylation levels for genome features between WT
14 (grey) and conditional *Dnmt1* cKO ESC induced for 1 day (dark red), 3 days (light red), 6
15 days (light pink), 9 days (light blue), 11 days (dark blue). Low methylated regions (LMRs)
16 (Stadler et al., 2011), enhancers defined by H3K4m1 (Chen et al., 2012) and H3K27ac
17 (Creyghton et al., 2010). Measurement of 2 biological replicates. For significance analysis
18 Wilcoxon rank sum test with Bonferroni correction testing with a p-value threshold of < 0.05.

19 (D) Chromosome view of RNA-seq reads over mRNA with Lx5 or MIRb TE sitting in the 2kb
20 surrounding region of a coding gene. RNA-seq libraries are strand specific. Each read is
21 depicted.

22 (E) Violin plots showing distribution of methylation levels for different TE classes between
23 WT (grey) and conditional *Dnmt1* cKO ESC induced for 1 day (dark red), 3 days (light red), 6
24 days (light pink), 9 days (light blue), 11 days (dark blue). Measurement of 2 biological
25 replicates. For significance analysis Wilcoxon rank sum test with Bonferroni correction testing
26 with a p-value threshold of < 0.05.

27 (F) Graphs showing methylation retention of TE classes in comparison to the rest of the
28 genome, (left) scatter plot of WGBS sequencing reads in gradient of grey with specific TE
29 class as red dot, (right) line graph of TE class in time course (red) in comparison to probes
30 starting with the same methylation level as the respective TE class (blue) and in comparison,
31 to the rest of the genome (grey). Measurement of 2 biological replicates.

32 (G) Scatter plot of all reads overlapping genes in the genome with the significantly *Dnmt1*
33 responsive genes highlighted in black. Significance was called by combining both Intensity
34 difference (SeqMonk) as well as DESeq2 significance called genes with a p-value threshold
35 of < 0.05 and multiple testing correction.

36 (H) Venn Diagram of the number and overlap of mRNAs upregulated upon *Dnmt1* cKO.

37 (I) Bar graph of 6 genes in WT which were most highly upregulated and downregulated upon
38 *Dnmt1* cKO induced 0 days (black), 1 day (dark red), 3 days (light red), 6 days (light pink), 9
39 days (light blue), 11 days (dark blue). Dots show the expression level in the 2 RNA-seq
40 libraries for each time point.

41 (J) Bar plots of expression of key pluripotency genes between WT (grey) and conditional
42 *Dnmt1* cKO ESC not induced (black), induced for 1 day (dark red), 3 days (light red), 6 days
43 (light pink), 9 days (light blue). Measurements of 2 biological replicate shown next to each
44 other.

45 (K) Bar plot showing percentage of genic insertions of *Dnmt1* and *Dicer* responsive TEs in
46 sense (red) and antisense (blue) direction to the respective genes.

47

48 **Figure S2. Genome wide small RNA response upon *Dnmt1* conditional KO, Related to Figure 2**

49 (A) Bar plots of small RNA size distribution as well as classification of different small RNA
50 classes in *Dnmt1* cKO and WT ESCs mapped to the whole genome; miRNAs (grey), rRNA
51 (green), small nuclear RNAs (snRNAs) (violet), miscellaneous other RNAs (misc RNAs)
52 (red), small nucleolar RNAs (snoRNA) (orange) and tRNA (light blue) of WT (right) and after
53 conditional *Dnmt1* cKO (left).

54 (B) Expression of endogenously transcribed miRNAs in WT (grey) and in conditional *Dnmt1*
55 cKO induced for 1 day (dark red), 3 days (light red), 6 days (light pink), 9 days (light blue), 11
56 days (dark blue). Error bars represent mean +/-SD of 3 technical replicates.

57 (C) Genic location of miRNA 200c with reads mapped in *Dnmt1* cKO and WT ESCs, each
58 line representing one read.

59 (D) Scatter plot of all small RNAs in the genome, highlighting miRNAs of the *Dlk* cluster
60 (black) and *Xlr3* cluster (green) at day 9 after *Dnmt1* cKO (y-axis) versus WT (x-axis).
61 Significance was called by combining both Intensity difference (SeqMonk) as well as
62 DESeq2 significance called genes with a p-value threshold of < 0.05 and multiple testing
63 correction.

64 (E) Bar graph of 2 representative small RNAs of the *Xlr3* and *Dlk* locus in WT and upon
65 *Dnmt1* cKO induced 1 day (dark red), 3 days (light red), 6 days (light pink), 9 days (light
66 blue), 11 days (dark blue). Error bars represent mean +/-SD of 3 technical replicates.
67 Statistics: two-sided Students t-test, * p-value <0.05, ** p-value <0.005, *** p-value <0.0005.

68 (F) Confirmation of small RNA-seq data by small RNA RT-qPCR, (left) Bar plot showing
69 small RNA RT-qPCR of mmu-miR-543 and mmu-miR-367 in WT (grey) and conditional
70 *Dnmt1* cKO induced for 9 days (dark red). Error bars represent mean +/-SD of 3 technical
71 replicates. Statistics: two-sided Students t-test, * p-value <0.05, ** p-value <0.005, *** p-
72 value <0.0005.

73 (G) Chromosome view of WGBS-seq, total RNA-seq and small RNA-seq depicted as wiggle
74 plots overlapping imprinted control regions (ICR), mRNA and small RNAs in WT and at day 9
75 after *Dnmt1* deletion.

76 (H) Pie chart distribution showing mapping of small RNA-seq from AGO2 IP 9 days after
77 conditional *Dnmt1* to different small RNA classes. miRNAs (black), repeats (dark green),
78 3'UTRs (yellow), introns (dark blue), piRNAs (light blue), 5'UTRs (light green), others (grey).

79 (I) Bar plot showing small RNA duplex 5' to 5' overlap of AGO2 IP small RNA-seq mapping to
80 repeats after conditional *Dnmt1* cKO induced 9 days.

81 (J) Bar plot showing nucleotide position 30 nt upstream and downstream of 5' end of AGO2
82 IP small RNA-seq libraries mapping to repeats after conditional *Dnmt1* cKO induced 9 days.

83 (K) Small RNA-seq of 20-24 nt small RNAs mapped to TEs *in vivo* PGCs of E13.5 as well as
84 E14.5 male (blue) and female (red) PGCs. Each library was done as 1 replicate.

85 (L) Pie chart distribution of small RNAs mapping to different genomic loci of *in vivo* E14.5
86 male PGC small RNA-seq libraries after conditional *Dnmt1* cKO induced 9 days. miRNAs
87 (black), repeats (dark green), 3'UTRs (yellow), introns (dark blue), 5'UTRs (light green),
88 rRNA_tRNA (grey), unannotated (white).

89 (M) Size distribution for *in vivo* E14.5 male PGCs of sense (blue) and antisense (red) small
90 RNAs mapping to repeatmasker consensus sequences using piPipes small RNA pipeline.

91 (N) Bar plot showing siRNA duplex 5' to 5' overlap for *in vivo* E14.5 male PGC small RNA-
92 seq libraries mapping to repeats.

93 (O) Bar plot showing nucleotide position 30 nt upstream and downstream of 5' end of *in vivo*
94 E14.5 male PGC small RNA-seq library mapping to repeats.

95

96 **Figure S3. Characterisation of the involvement DICER and AGO2 in TE silencing, Related to Figure 3**

97 (A) (left) Schematic showing *Dicer* conditional cKO generation using CRISPR by introducing
98 loxP sites into Intron 14_15 and Intron 20_21. Agarose gel of PCR to screen for genomic
99 recombination of 2 *Dicer/Dnmt1* conditional double cKO clones after addition of 4OHT for 3
100 days. Recombination of Intron 15-16 was tested with primer set 1, recombination of intron
101 20-21 was tested with primer set 2 and recombination of both introns was tested with primer
102 set 3, LD = 1000 bp DNA ladder. (middle) RT-qPCR of *Dicer* mRNA upon CRE
103 recombination induced by tamoxifen (4OHT) in clone 1 (light green) and clone 2 (dark green)
104 of *Dicer* conditional KO ESCs. Error bars represent mean +/-SD of 3 technical replicates.
105 Statistics: two-sided Students t-test, * p-value <0.05, ** p-value <0.005, *** p-value <0.0005.
106 (right) RT-qPCR of *mmu-miR-93* expression in ESCs upon *Dicer* KO in clone 1 (light green)
107 and clone 2 (dark green) controlled by snoRNA expression. Error bars represent mean +/-SD
108 of 3 technical replicates. Statistics: two-sided Students t-test, * p-value <0.05, ** p-value
109 <0.005.

110 (B) Bar graph of percentage of genic antisense transcription over the time course of
111 *Dicer/Dnmt1* cDKO, *Dicer* KO and *Dnmt1* cKO in KO over WT samples. Measurement of 2
112 biological replicates for *Dicer/Dnmt1* cDKO and *Dnmt1* cKO and WT samples and 1 replicate
113 for *Dicer* KO ESCs.

114 (C) Bar plots of small RNA size distribution as well as classification of different small RNA
115 classes in *Dicer/Dnmt1* cDKO, *Dnmt1* cKO with KO induced for 4 days and *Dnmt1*^{f/f} mESCs
116 and WT mapped to the whole genome; miRNAs (light blue), rRNA (grey), small nuclear
117 RNAs (snRNAs) (dark blue), miscellaneous other RNAs (misc RNAs) (orange), small
118 nucleolar RNAs (snoRNA) (yellow) and tRNA (light green).

119 (D) Small RNA-seq of *Dicer/Dnmt1* cDKO and *Dnmt1* cKO ESCs normalised to WT ESCs
120 mapped to IAPEz and L1MdGf TE classes. *p<0.05, **p<0.005, two-tailed student t-test.
121 Measurement of 2 biological replicates.

122 (E) Schematic showing *Ago2* conditional cKO generation using CRISPR by introducing loxP
123 sites into Intron 8_9 and Intron 11_12 of *Ago2* mRNA. Agarose gel of PCR to screen for
124 genomic recombination of four *Ago2/Dnmt1* conditional double cKO clones after addition of
125 4OHT for 3 days in comparison to one WT clone. Recombination of Intron 8-12 was tested
126 with primer set 1. LD = 100 bp DNA ladder.

127 (F) RT-qPCR analysis of *Ago2* in ESCs following conditional *Ago2/Dnmt1* cDKO by
128 treatment with 4OHT or control (EtOH) for 3 days. Error bars represent mean +/-SD of 3
129 biological replicates in 3 technical replicates. Values were normalized to Hspcb and
130 controlled to EtOH samples. Statistics: two-sided Students t-test, * p-value <0.05, ** p-value
131 <0.005.

132 (G) Immunofluorescence of AGO2 protein (purple) in *Ago2/Dnmt1* cDKO and *Dnmt1* cKO
133 ESCs upon KO induction with 4OHT. Deletion was induced for 3 or 8 days as depicted.
134 Nuclear DAPI counter staining (white). scale bar = 20µm.

135 (H) (upper panel) Schematic knock out strategy for *Dicer* in mouse ESCs constructing
136 gRNAs against Exon 23 and 24 of *Dicer* mRNA. gRNA Protospacer Adjacent Motif (PAM)
137 sequences (dark blue). (Bernstein et al., 2003), (lower left) RT-qPCR of mRNA expression of
138 *Dicer* in WT (black) and *Dicer* cKO (dark blue). Error bars represent mean +/-standard
139 deviations of 3 technical replicates. Statistics: two-sided Students t-test, * p-value <0.05, **
140 p-value <0.005, *** p-value <0.0005, (lower right) Expression level of *mmu-miR-93* in
141 wildtype (black) and *Dicer* cKO (dark blue). Error bars represent mean +/-standard deviations
142 of 3 technical replicates. Statistics: two-sided Students t-test, * p-value <0.05, ** p-value
143 <0.005, *** p-value <0.0005,

144 (I) (upper panel) Schematic of knock out strategy for *Ago2* in mouse ESCs constructing
145 gRNAs against Intron 13-14 and 115 of *Dicer* mRNA. gRNA PAM sequences (light green).
146 (lower panel) RT-qPCR of *Ago2* expression in 2 clones of *Ago2* KO ESCs (dark purple) in

147 comparison to *Dnmt1*^{fl/fl} ESCs (black). Error bars represent mean +/-standard deviations of 3
148 technical replicates. Statistics: two-sided Students t-test, * p-value <0.05, ** p-value <0.005,
149 *** p-value <0.0005,
150 (J) Immunofluorescence of AGO2 protein (purple) and NANOG (green) in *Ago2* KO/*Dnmt1*
151 cKO and mouse embryonic fibroblasts. Nuclear DAPI counter staining (white). scale bar =
152 20µm. Differences of *Ago2* KO versus WT were analysed using FIJI and manual ROIs to
153 semi-quantify the *Ago2* signal intensity in the cells. The mean intensity (to correct for different
154 cell size) was analysed and statistically significant was calculated in GraphPad (Students t-
155 test, p-value <0.0005).
156 (K) Bar plots of expression of 5 pluripotency genes between WT (grey) and conditional
157 *Dnmt1* cKO ESC induced for 11 days (dark blue), *Dicer* KO (light blue) treated with EtOH for
158 1 day and 11 days, *Dicer* KO/*Dnmt1* DKO (faint blue) treated with 4OHT for 1 and 11 days.
159 (L) Scatter plot of RNA-seq data of *Dicer* KO (y-axis) versus WT (x-axis) ESCs. Differentially
160 expressed genes were called by intensity difference of SeqMonk (black), all other genes are
161 depicted in grey.
162 (M) Chromosome view of read count quantitation across the 4 genes *Lin28*, *Dnmt3l*, *Fbln2*
163 and *Oct4*. High bars indicated high expression, low bars indicate low expression. Every bar
164 overlaps at least 1 read.
165 (N) RT-qPCR data of LINE and major satellites in *Dicer* KO/*Dnmt1* cKO following conditional
166 *Dnmt1* cKO, by treatment with 4OHT. Error bars represent SD of 3 technical replicates.
167 Values were normalized to *Atp5b*, *Hspcb* and Major satellites to U1. Error bars represent
168 mean +/-standard deviations of 3 technical replicates. Statistics: two-sided Students t-test, *
169 p-value <0.05, ** p-value <0.005, *** p-value <0.0005,
170 (O) Heatmap of unbiased hierarchical clustering of all TE classes responsive *Dicer*
171 KO/*Dnmt1* cKO versus *Dnmt1* cKO. Heatmap is showing relative expression (z-score) of TEs
172 upon *Dnmt1* cKO and were generated using the pheatmap R library.

173

174 **Figure S4. Distribution of repressive histone marks – H3K9me3, H3K9me2 and H3K27me3 in ESCs**
175 **upon *Dnmt1* cKO, Related to Figure 4**

176 (A) Pie chart of enrichment of H3K27me3, H3K9me3 and H3K9me2 in repeats (dark violet),
177 genic regions (light violet), promoters (dark green), CGIs (middle green), intergenic regions
178 (light green) in wildtype ESCs.
179 (B) Probe enrichment of H3K9me3 (green), H3K9me2 (yellow) and H3K27me3 (blue) over
180 gene body and TSS.
181 (C) Aligned probe plot of H3K27me3 enrichment surrounding 5kb of TSS.
182 (D) Scatter plot of repressive histone marks overlapping genes in wildtype (y-axis) versus
183 *Dnmt1* cKO (x-axis) ESCs.

184 (E) Wiggle plot of ChIP enrichment of H3K9me3 (green), H3K27me3 (blue) and H3K9me2
185 (yellow) over a 500kbp region in Chromosome 12. Intensity of the enrichment on the y-axis.
186 (F) Wiggle plot of H3K9me3 enrichment over IAPEZ in *Dnmt1* cKO at day 4 (red), day 8
187 (blue) and in WT (grey). Plots were generated using SeqMonk wiggle-plot quantitation.
188 (G) Bar graph of enrichment of H3K27me3, H3K9me3 and H3K9me2 in repeats (dark violet),
189 genic regions (light violet), promoters (dark green), CGIs (middle green), intergenic regions
190 (light green) in WT ESCs, *Dnmt1* cKO, *Dicer* KO and *Dicer/Dnmt1* cDKO
191 (H) Wiggle plot of ChIP-seq enrichment of H3K9me3, H3K27me3 and H3K9me2 at three
192 genomic loci in *Dicer/Dnmt1* cDKO at day 11 (light blue), *Dicer* KO (middle blue), *Dnmt1* cKO
193 at day 11 (dark blue) and WT (grey). Enrichment intensity shown on y-axis.
194 (I) Summary of TE classes across WGBS-seq, RNA-seq, small RNA-seq and ChIP-seq
195 libraries. Scale from red (loose) to green (gain).

196

197

198 **Supplemental Tables**

199 ***Table S1: List of differentially expressed genes upon *Dnmt1* KO and *Dicer* KO, Related to Figure 1***
200 ***and S1 and Figure 3 and S3.***

201 Differentially expressed genes were called using the overlap between the SeqMonk Intensity
202 difference as well as DESeq2.

203

204 ***Table S2: RT-qPCR primers, Related to Figure 3 and S3***

205 Primers below have been used for expression analyses (RT-qPCR primers).

206

207 ***Table S3: CRISPR primers, Related to Figure 3, S3***

208 CRISPR primers were used to construct *Dicer* KO/*Dnmt1* cKO and *Dicer/Dnmt1* cDKO, *Ago2*
209 KO/*Dnmt1* cKO and *Ago2/Dnmt1* cDKO mouse ES cells. gRNA (guide RNA).

210

211 **Supplemental Data**

212 Data S1: Raw code to analyse TEs, Related to Figure 1-4.

213

214

215

216

217

Figure S2

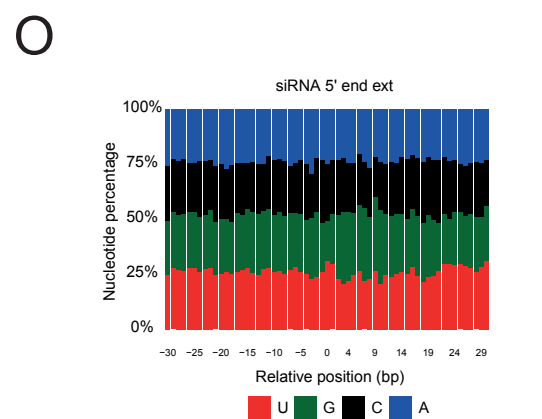
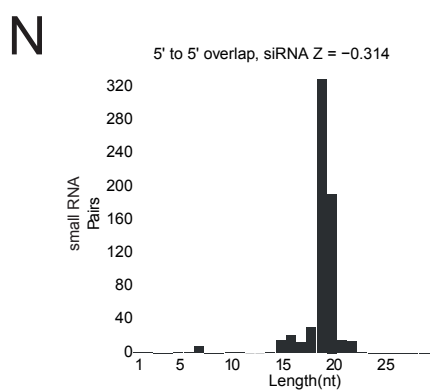
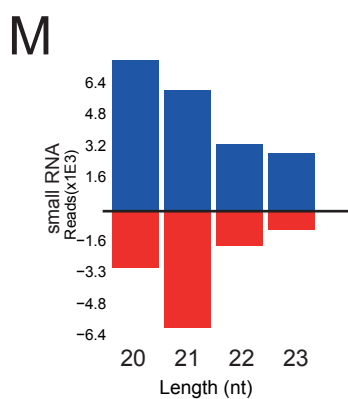
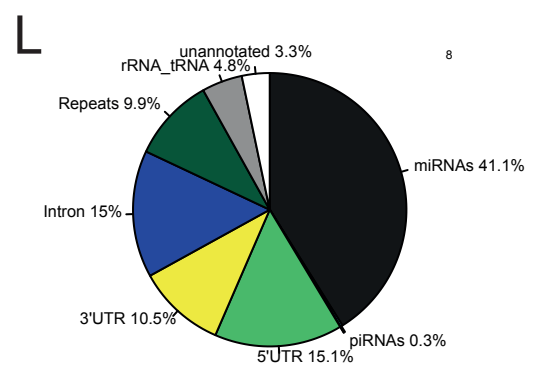
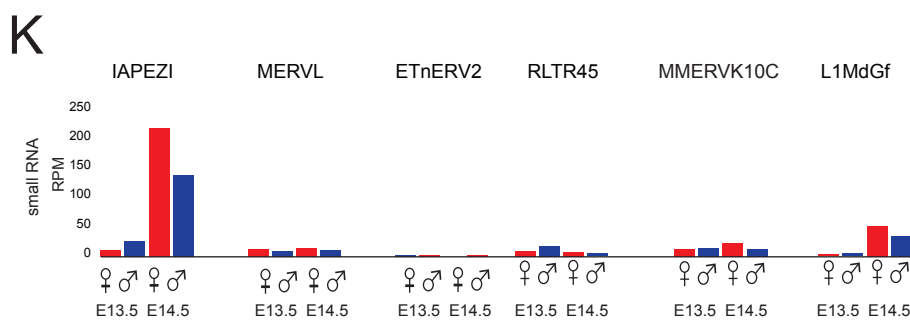
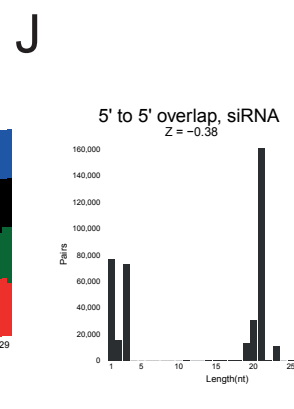
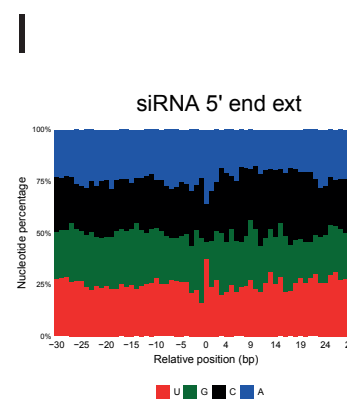
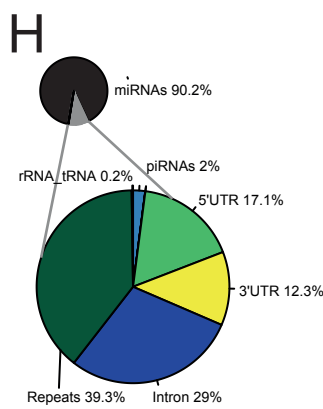
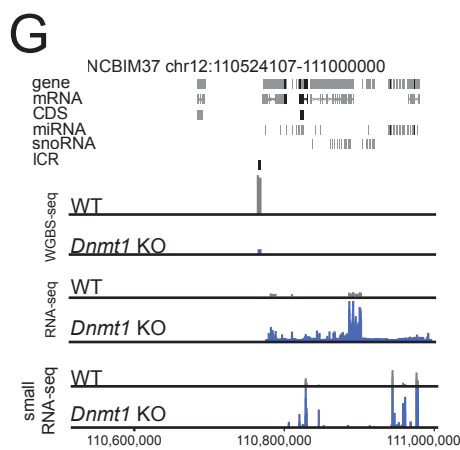
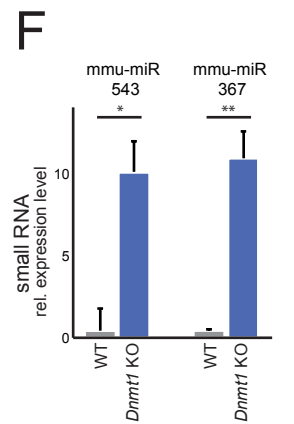
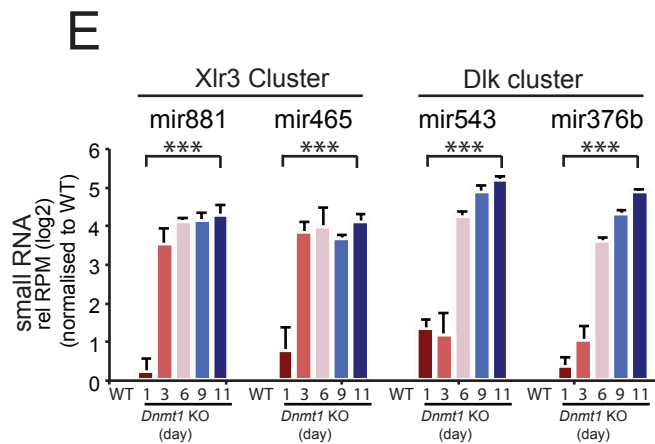
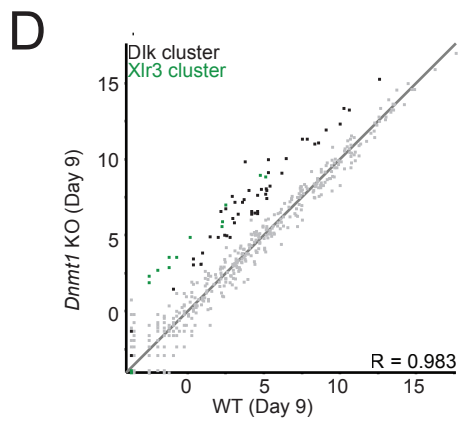
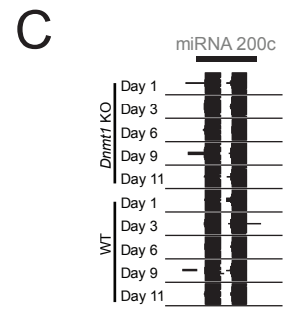
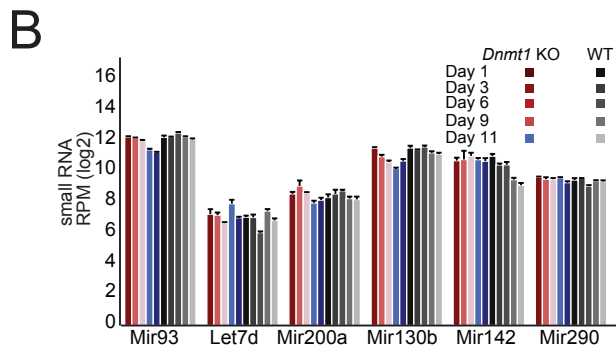
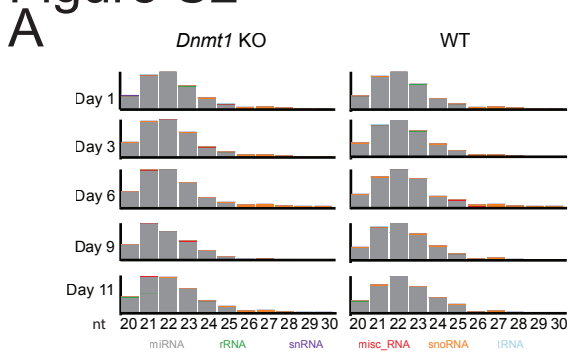


Figure S3

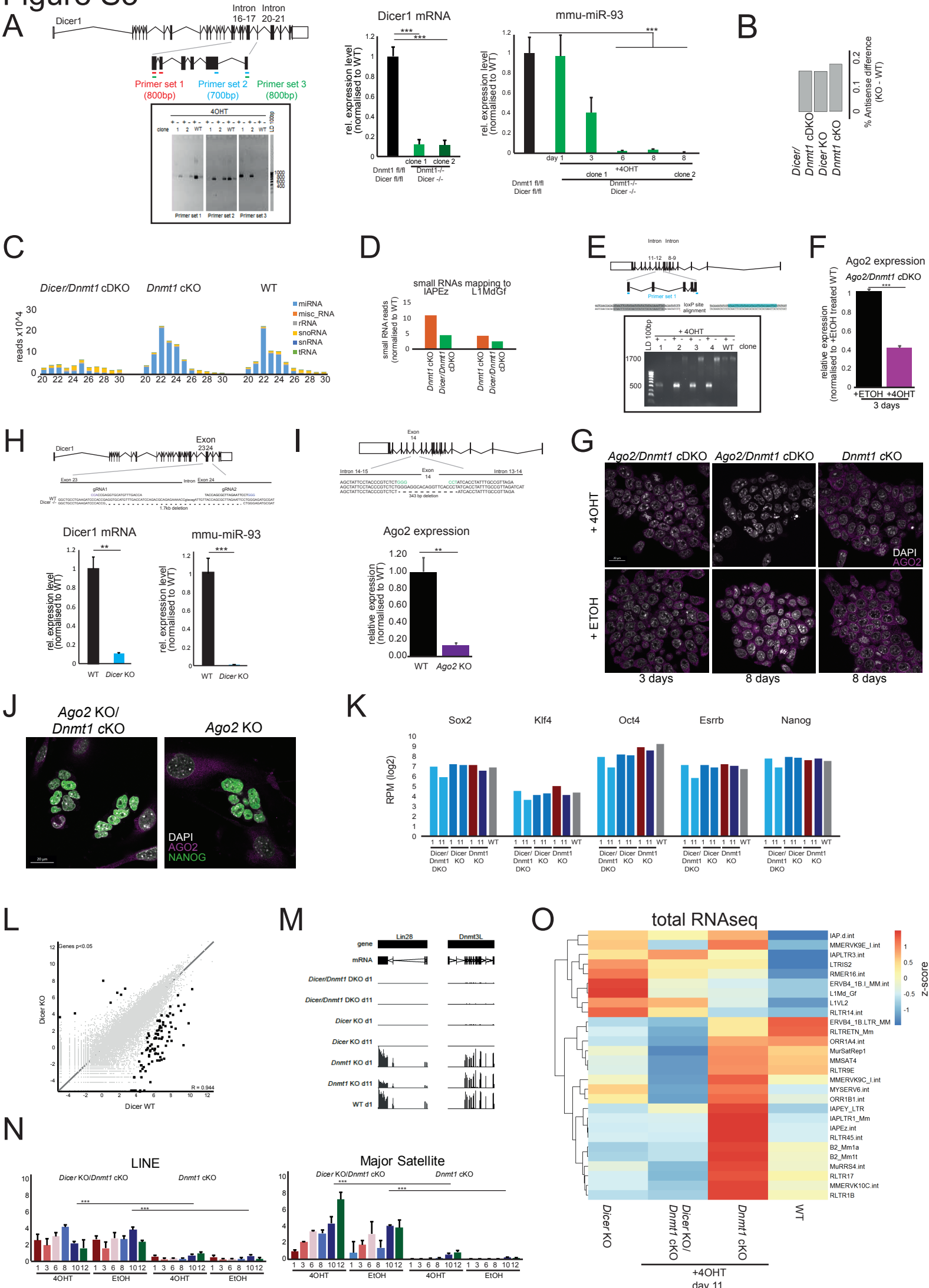
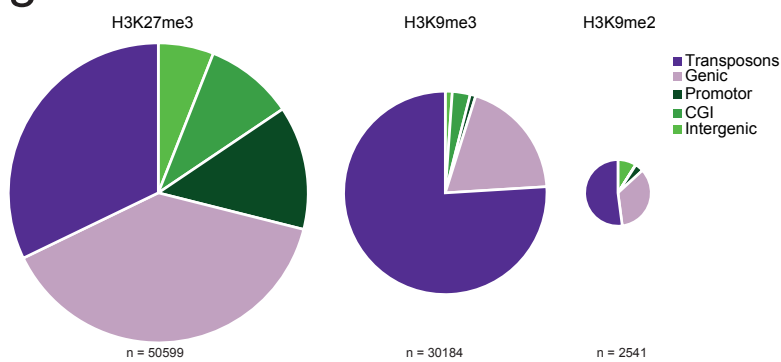
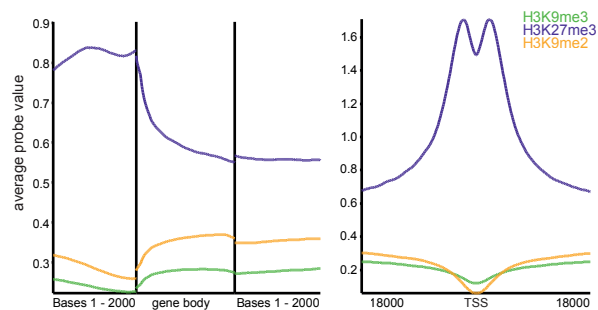


Figure S4

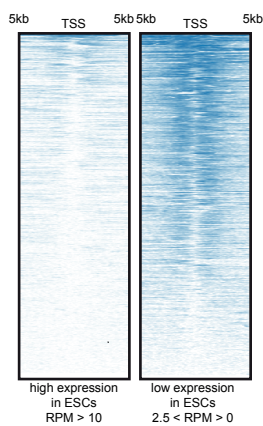
A



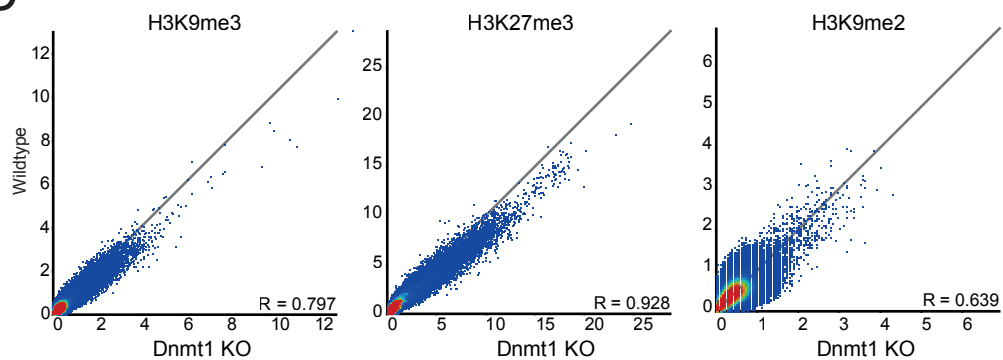
B



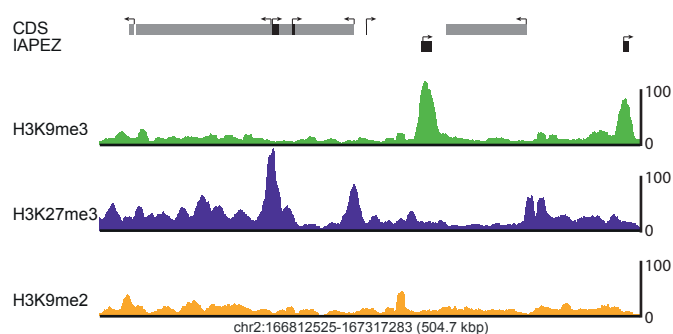
C



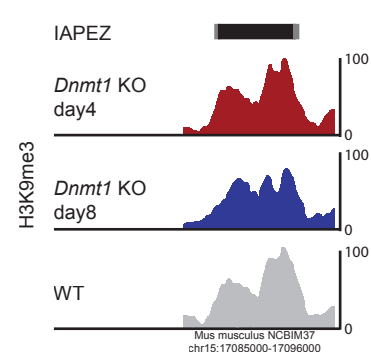
D



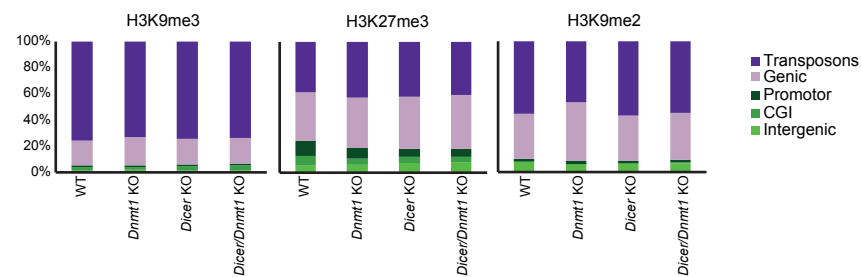
E



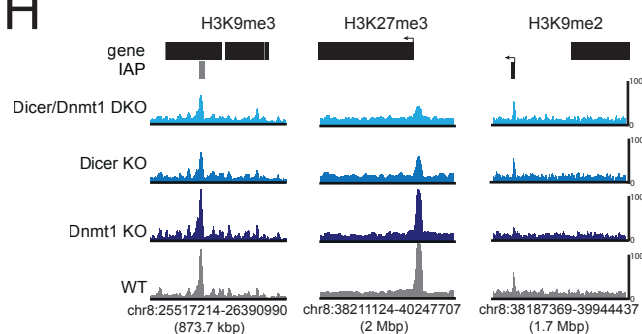
F



G



H



I

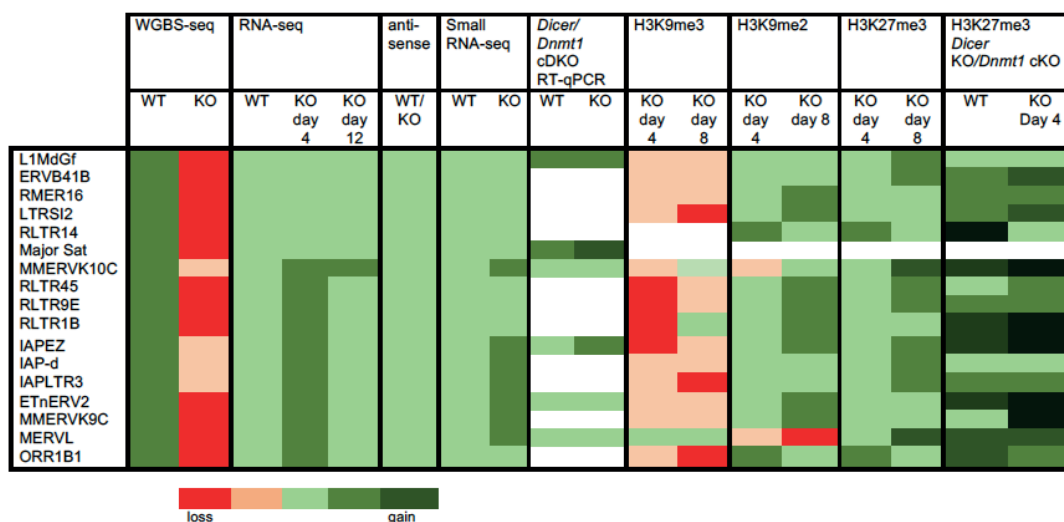


Table S2: RT-qPCR primers, Related to Figure 3 and S3

Gene	Primer	Sequence	origin
Hspcb	msRT_Hspcb_FW	GCTGGCTGAGGACAAGGAGA	
	msRT_Hspcb_RV	CGTCGGTTAGTGGAACTTTCATG	
Atp5b	msRT_Atp5b_FW	GGCCAAGATGTCCTGCTGTT	
	msRT_Atp5b_RV	GCTGGTAGCCTACAGCAGAAGG	
Dicer	Dicer_RT_17_18_FW	GCATTCCTAGCACCAAGTATTCA	This study
	Dicer_RT_17_18_RV	GGAAGGAAATTTACTGAGTGGGG	This study
	Dicer_RT_FW	GAACGAAATGCAAGGAATGGA	
	Dicer_RT_RV	GGGACTTCGATATCCTCTTCTTTCTC	
Ago2	Eif2c2_FW	GCCGTCCTTCCCCTACCAC	
	Eif2c2_RV	GGTATTGACACAGAGCGTGTGC	
Dgcr8	Dgcr8_FW	CCTAAAGACAGTGAAGAACTGGAGTA	
	Dgcr8_RV	CATGGAGGATCTGATATGGAGAC	
IAP	IAP_Nature_qPCR_FW	AAGCAGCAATCACCCACTTTGG	(ref)
	IAP_Nature_qPCR_RV	CAATCATTAGATGTGGCTGCCAAG	(ref)
MERVL	MuERV-L gag_Jafar_FW	TTCTTCTAGACCTGTAACCAGACTCA	(Sharif et al., 2016)
	MuERV-L gag_Jafar_RV	TCCTTAGTAGTGTAGCGAATTTCTC	(Sharif et al., 2016)
Etn	MusD_Nature_qPCR_FW	GTGGTATCTCAGGAGGAGTGCC	
	MusD_Nature_qPCR_RV	GGGCAGCTCCTCTATCTGAGTG	
U1	U1_AP_FW	CTTACCTGGCAGGGGAGATA	
	U1_AP_RV	CAGTCCCCCACTACCACAAA	
Maj. Sat.	MajSat_BL_FW	GACGACTTGAAAAATGACGAAATC	
	MajSat_BL_RV	CATATTCCAGGTCCTTCAGTGTGC	
MMERVK10C	MmERVK10C_FW	ATGTGAGCTAGCTGTTAAAGAAGGAC	
	MmERVK10C_RV	CTCTCTGTTTCTGACATACTTTCCTGT	
LINEI	LINE ORF2_JS_FW	GACATAGACTAACAACTGGCTACACAAAC	(Sharif et al., 2016)
	LINE ORF2_JS_RV	GGTAGTGTCTATCTTTTTCTCTGAGATGAG	(Sharif et al., 2016)

Table S3: CRISPR primers, Related to Figure 3 and S3

Gene	Primer	Sequence (5'-3')	
U6	U6-Fwd	GAGGGCCTATTTCCCATGATTCC	PCR screen
<i>Dicer</i> KO / <i>Dnmt1</i> cKO	Dicer1_X23_gRNA_FW	CACCGAGTAATCAAAAGGACCAGCC	gRNA
	Dicer1_X23_gRNA_RV	AAACGGCTGGTCCTTTTGATTACTC	gRNA
	Dicer1_X24_gRNA_FW	CACCGTTACCAGCGCTTAGAATTCC	gRNA
	Dicer1_X24_gRNA_RV	AAACGGAATTCTAAGCGCTGGTAAC	gRNA
	Dicer_23_24_screen_FW	AGCAGTGCATTGCTGACAAGAG	PCR screen
	Dicer_23_24_screen_RV	CTTGTGGTAGTCATACTTCACAGCC	PCR screen
<i>Dicer/Dnmt1</i> cDKO	Dicer_14_15_gRNA_FW	CACCGCACTCAGCATCGAGTCTCG	gRNA
	Dicer_14_15_gRNA_RV	AAACCGAGACTCGATGCTGAGTGCC	gRNA
	Dicer_20_21_gRNA_FW	CACCGAGCAATGATCCGGTCTCAGG	gRNA
	Dicer_20_21_gRNA_RV	AAACCCTGAGACCGGATCATTGCTC	gRNA
	Dicer_14_15_RV1	TGAAACCAGACTTCTTCAGCTCG	PCR screen
	Dicer_14_15_FW1	CCTTTCCTCTTGACATTTACCT	PCR screen
	Dicer_2021_FW1	GGTGTCAGATCACTTCCCCT	PCR screen
	Dicer_2021_RV1	TGACCAGAATAAGAAGGAGCGGA	PCR screen
	Dicer_20_21_donor_loxP	gacaaggaccactgtactgtttatccctgaagtagcagactagacca ttgagatctgtcaagttagagagcagcaagaattctATAACTTC GTATAGCATACATTATACGAAGTTATgagaccggat cattgctcctgtagcagtgatgctggaataggggtgagaatggatata gttcttctcaaaactaa	Donor DNA
Dicer_14_15_donor_loxP	ggcaagaaaagacatttattctggttggtgggtaacaaagcagc agcagcagctcagaaggcactcagcatcgagtctATAACTTC GTATAATGTATGCTATACGAAGTTATcgatcgaagc cagagctgcacactgcccaattttacctatgctgcttattacagtttatg gaatatcaaaagtatttaaaatag	Donor DNA	
<i>Ago2</i> KO/ <i>Dnmt1</i> cKO	Ago2_13_14_gRNA_FW	CACCGCTGGTCTAATCATGATCTAA	gRNA
	Ago2_13_14_gRNA_RV	AAACTTAGATCATGATTAGACCAGC	gRNA
	Ago2_14_15_gRNA_FW	CACCGAAGCTATTCTACCCGTCTC	gRNA
	Ago2_14_15_gRNA_RV	AAACGAGACGGGTAGGAATAGCTTC	gRNA
	Ago2_13_14_FW	AGGCTACCTTGATGGACATGG	PCR screen
	Ago2_14_15_RV	GATGGGTTTGGTGGTACATGC	PCR screen
<i>Ago2/Dnmt1</i> cDKO	Ago2_8_9_gRNA_FW	CACCGGTTACCTACAAGTTGTGTG	gRNA
	Ago2_8_9_gRNA_RV	AAACCACACAACCTGTAGGTAACC	gRNA
	Ago2_11_12_gRNA_FW	CACCGGTTGGTCAGACGGGTCACCG	gRNA
	Ago2_11_12_gRNA_RV	AAACAGGGTGACTGCCATTTATGAC	gRNA
	Ago2_8_9_FW	CCTGCTCTTCTGGAGGCATTT	PCR screen
	Ago2_8_9_RV	CCTGCTCTTCTGGAGGCATTT	PCR screen
	Ago2_11_12_FW	GTCCAGGGTGTGTGGGACAT	PCR screen
	Ago2_11_12_RV	GCAACTTCCTCAGCTAATCCTCCA	PCR screen
	Ago2_8_9_donor_loxP	ctcactgtgcacaggtaagcccagcagagtgccaccaagctgta gatggctcttcatgccagggttacctacaagAtAtCgtATAAC TTCGTATAGCATACATTATACGAAGTTATgtgtggtt gacttggagtggtcccaccactagtcagggttggtctggtctgcta ctcagcctctgaaatctcct	Donor DNA
Ago2_11_12_donor_loxP	tgttggtcagacgggtcaccgggttccaataccagcggttggcagc cttctctaacagagagcactcaccaggATAACTTCGTATA GCATACATTATACGAAGTTATgAAITCgactgcccattt atgagatgtgacaaggccagattaggtgtgagagaaaacagctct gagactgtagaactcactgtctat	Donor DNA	



Click here to access/download

Supplemental Movies and Spreadsheets
Table_S1.xlsx



